A novel ferroptosis-related gene signature can predict prognosis and influence immune microenvironment in acute myeloid leukemia

Xianbo Huang#, De Zhou#, Xiujin Ye*, Jie Jin*

ABSTRACT

Acute myeloid leukemia (AML) is a highly heterogeneous hematopoietic malignancy that strongly correlates with poor clinical outcomes. Ferroptosis is an iron-dependent, non-apoptotic form of regulated cell death which plays an important role in various human cancers. Nevertheless, the prognostic significance and functions of ferroptosis-related genes (FRGs) in AML have not received sufficient attention. The aim of this article was to evaluate the association between FRGs levels and AML prognosis using publicly available RNA-sequencing datasets. The univariate Cox regression analysis identified 20 FRGs that correlate with patient overall survival (OS). The LASSO Cox regression model was used to construct a prognostic 12-gene risk model using a TCGA cohort, and internal and external validation proved the signature efficient. The 12 FRGs signature was then used to assign patients into high- and low-risk groups, with the former exhibiting markedly reduced OS, compared to the low-risk group. ROC curve analysis verified the predictive ability of the risk model. Functional analysis showed that immune status and drug sensitivity differed between the two risk groups. In summary, FRGs is a promising candidate biomarker and therapeutic target for AML.

KEYWORDS: Acute myeloid leukemia; ferroptosis; prognostic gene signature; overall survival; tumor immune microenvironment; drug resistance

INTRODUCTION

Acute myeloid leukemia (AML), the most prevalent leukemia in adults, is a heterogeneous malignancy that arises from clonal expansion of transformed pluripotent hematopoietic stem cells. It is associated with various genomic alterations [1,2]. Efforts have been aimed at elucidating the genetic landscape of AML, however, the current therapeutic options, including allogeneic hematopoietic stem cell transplantation and intensive chemotherapy, have not led to significant improvements in clinical outcomes [3,4]. Majority of

Department of Hematology, The First Affiliated Hospital, College of Medicine, Zhejiang University, Hangzhou, China

*Corresponding authors: Jie Jin, Department of Hematology, The First Affiliated Hospital, College of Medicine, Zhejiang University, No.79 Qingchun Road, Shangcheng District, Hangzhou City, Zhejiang Province, China. E-mail: yxjsunny@zju.edu.cn
Xiujin Ye, Department of Hematology, The First Affiliated Hospital, College of Medicine, Zhejiang University, No.79 Qingchun Road, Shangcheng District, Hangzhou City, Zhejiang Province, China. E-mail: jiej0503@zju.edu.cn
#These authors contributed equally to the work.

AML patients suffer relapse while overall survival (OS) rate remains <30% [4]. Thus, a better understanding of the molecular basis of AML may identify novel diagnostic and prognostic biomarkers of AML, as well as therapeutic targets for better outcomes.

Apoptosis induction by chemotherapy is a key mechanism underlying leukemia cell death [5]. However, relapsed/refractory AML is often resistant to apoptosis [6,7], calling for novel ways of inducing cell death. Ferroptosis, a form of regulated cell death (RCD), has recently been reported. It is iron dependent and differs from apoptosis, autophagy, necrosis, necroptosis, pyroptosis, and other cell death forms [8]. It is defined by cell membrane ruptures and blisters, shrinkage of the mitochondrial, enhanced membrane density, decrease or vanishing of mitochondrial ridges, outer mitochondrial membrane rupture, and nuclei that are normal sized but lacking condensed chromatin. Ferroptosis is triggered by accumulation of iron, excess reactive oxygen species (ROS) levels, and high lipid peroxidation levels [9,10]. A set of genes, which are associated with various metabolic changes, have been shown to regulate ferroptosis. Several pathways, including mevalonate and iron, lipid, as well as glucose metabolism, are involved in ferroptosis. Glutathione peroxidase 4 (GPX4) and cystine-glutamate antiporter (system XC-) are crucial ferroptosis pathway components. Iron uptake and use are vital for ferroptosis [11,12].

Dysregulation of ferroptosis is observed in a wide range of disorders, including cancer. Ferroptosis induction is a likely therapeutic avenue for triggering cancer cell death, particularly for

tumors with resistance to traditional therapies [13,14]. Ferroptosis has important roles in AML. Upregulation of GPX4, a phospholipid (PL) hydroperoxidase that negatively regulates ferroptosis, correlates with poor AML prognosis [15]. Aldehyde dehydrogenase 3a2, a long-chain aliphatic aldehyde-oxidizing enzyme, protects AML cells from oxidative death and is highly lethal with GPX4 suppression-mediated ferroptosis [16]. APR-245 (p53-mutated protein inhibitor) [17], ATPR (a novel all-trans retinoic acid derivative) [18], FTY720 (sphingosine-1-phosphate inhibitor) [19], typhaneoside [20], and dihydroartemisinin (DHC) [21] can induce ferroptosis in AML cells. However, the molecular basis of ferroptosis and its role in AML prognosis is unclear.

Here, we elucidate on the features of ferroptosis-related genes (FRGs) in AML using publicly available AML RNA-seq data and the equivalent clinical data. We then constructed a prognostic 12 FRGs risk signature using the TCGA cohort and validated it on GEO datasets. Functional analyses were conducted to elucidate on the pathomechanisms. Our findings show the ferroptosis prognostic landscape, which has potential application in predicting AML prognosis.

MATERIALS AND METHODS

Data collection from publicly available databases

RNA-seq data belonging to 151 AML patients were obtained from TCGA (https://portal.gdc.cancer.gov/). After exclusion of samples that lacked corresponding clinical data, data on 130 AML samples remained for analysis. In addition, the Series Matrix File of dataset GSE71014 was retrieved from GEO (https://www.ncbi.nlm.nih.gov/geo/). Then, the platform's gene probes were transmuted into gene names through referencing the GPL10588 platform. Next, data on 104 AML patients who had complete gene expression profiles as well as survival data were retrieved. The Series Matrix File for dataset GSE12417 (annotation platform: GPL570) containing data on 78 AML patients who had complete gene expression profiles as well as survival data was also retrieved. A total of 103 FRGs were retrieved from GeneCards (https://www.genecards.org/) and BioGPS (http://www.biogps.org/). We then extracted the shared FRGs from the three datasets (TCGA-LAML, GSE71014, and GSE12417) and excluded poorly expressed genes whose value was "0" in over half of the samples, or had "<0.3" as the mean value of expression.

Functional annotation of AML-related FRGs

Survival analysis was conducted on AML-related FRGs. Univariate Cox evaluation of OS was done to establish FRGs with prognostic value, with $p < 0.05$ indicating statistical significance. Functional analysis of the AML-related FRGs using

gene ontology (GO) and Kyoto Encyclopedia of Genes and Genomes (KEGG) analyses was done through "clusterProfiler" in R [22]. Cutoff p- and p-values were set at 0.05.

Establishment and verification of a prognostic FRGs signature

To minimize overfitting risk, least absolute shrinkage and selection operator (LASSO)-penalized Cox regression analyses were conducted to establish candidate genes for use in the risk score signature. Risk features for prognosis were evaluated using "glmnet" and "survival" packages on R using LASSO [23]. We used a k-fold ($k = 10$) cross-validation in the LASSO regression. The dataset was randomly divided into 10 individual subjects, and the ratio of training and validation sets was 9:1. We trained the models with k–1(9) folds and validated them with the rest one. In the regression analysis, the normalized expression matrix of candidate prognostic FRGs was used as the independent variable. AML OS for the TCGA cohort was the response variable. Finally, 12 candidate FRGs were selected and entered further analysis. Calculation of AML patients' AML risk scores was based on normalized levels for every FRG and its regression coefficients using the formula: Score = sum (corresponding coefficient × each gene's expression). The median risk score was used to stratify patients into low- and high-risk groups. Two-sided log-rank tests and Kaplan–Meier survival analyses were performed to determine differences in OS between the two groups. LASSO analysis was used to test the risk score's capacity for prognostic prediction. Receiver operating characteristic (ROC) curve analysis assessed the model's prognostic accuracy.

Prediction of clinical chemotherapeutic response

Next, we used the "pRRophetic" [24] package on R to predict clinical chemotherapeutic response for every AML patient in the above cohort based on the Genomics of Drug Sensitivity in Cancer (GDSC) database (https://www.cancer-rxgene.org/). The projected IC_{50} for every cell line exposed to a particular drug was acquired through ridge regression, while predictive accuracies were determined through 10-fold cross-validation using the GDSC training set. For all parameters, including "combat," default values were obtained for removal of batch effect and mean value for summarizing duplicate gene expression [25].

Evaluation of tumor-infiltrating immune cells (TIICs)

CIBERSORT (https://cibersort.stanford.edu/) is an algorithm for analyzing RNA expression data and determining the proportions of various cell subtypes in every sample [26]. Next, we used CIBERSORT to determine the proportion of TIICs in

the subgroups of AML samples. CIBERSORT offers R language computing source code and LM22 signature gene matrix [26]. The R programs comprise "preprocessCore" and "e1071" packages. In the R program, 1000 (recommended value is >100) was set as the statistical rank while quantile normalization was disabled. Next, the ratios for relative infiltrations of 22 distinct immune cell types were evaluated, with 1 as the sum of fractions. Spearman correlation analysis using "cor.test" in R was used to evaluate associations between infiltrations of immune cells and gene expressions. $p < 0.05$ was the cutoff for significance.

Gene set enrichment analysis (GSEA)

GSEA (https://www.broadlnstitute.org/gsea/) was used to identify differential expressions of genes (gene sets) that were functionally related and whose enrichment in AML patient subgroups was significant [27]. GO and KEGG pathway databases, which were used as functional enrichment reference sets, were obtained from the Molecular Signatures Database [28]. Minimal and maximal gene set sizes were set at 20 and 500, respectively. GSEA performed 1000 permutation, and gene sets with $p < 0.05$ and false discovery rate ≤0.25 were significant. Finally, markedly enriched KEGG pathways and GO terms are concentratedly displayed.

Tumor-immune interaction analysis

Tumor-Immune System Interactions Database (TISIDB; http://cis.hku.hk/TISIDB/index.php) is an integrated repository of data from several databases, including TCGA, UniProt, DrugBank, and GO, and is used to assess tumor-immune associations across human cancers [29]. We used TISIDB to assess the relationship between TIIC-related signatures and expression levels of FRGs included in the prognostic risk score model using Spearman's test. $p < 0.05$ was the cutoff for significance and all tests were two sided. These findings were presented on heatmaps developed using "pheatmap" in R.

Statistical analysis

Analyses were done using R v3.6 (www.r-project.org). Based on the FRGs signature, two-sided log-rank tests and Kaplan–Meier survival analyses were conducted to determine OS differences between high- and low-risk group patients. A Cox proportional hazards regression model was used for multivariate analysis. ROC curve analysis using "pROC"in R was used for OS prediction. Associations between clinical variants and the risk score were evaluated by the Chi-square test. $p < 0.05$ denoted significance.

RESULTS

Figure 1 shows the schematic presentation of this study. One hundred and thirty AML patients from the TCGA-LAML cohort were recruited in this study and their clinical features are shown in Table 1.

Prognostic FRGs in AML patients

Gene expression data for the AML cohort were retrieved from TCGA as well as FRGs expression patterns extracted from the dataset. On exclusion of poorly expressed genes with a value of "0" in over half the samples, or <0.3 as the mean expression value, 94 FRGs remained for analysis (Table S1). Univariate Cox regression survival analysis on the 94 FRGs identified 20 that significantly correlated with AML prognosis (all $p < 0.05$, Figure 2A). Interactions among these genes are presented in Figure 2B. Detailed information on the 20 AML-related FRGs is shown on Table S2.

Functional analysis of the AML-associated FRGs

For the 20 FRGs, GO analysis of biological processes (BP) found that these genes were most enriched in cell responses to external stimulus, oxidative stress responses, and nutrient level responses. With regard to cellular component, these genes were highly enriched in the outer membrane of the

TABLE 1. Clinical characteristics of AML patients in TCGA cohort

Discrete variables	Number	Percentage
Gender		
Male	60	46.15
Female	70	53.85
Fab subtype		
M0	12	9.23
M1	30	23.08
M2	32	24.62
M3	14	10.77
M4	27	20.77
M5	12	9.23
M6	2	1.54
M7	1	0.77
Karyotype		
Favorable	30	23.08
Intermediate	72	55.38
Poor	26	20.00
Unknown	2	1.54
Gene mutation		
Positive	66	50.77
Negative	64	49.23
Living status		
Dead	78	60.00
Alive	52	40.00
	Range	Median
Continuous variables		
Age (years)	21-88	56
Overall survival (days)	28-2861	366
White blood cell (10×9/L)	1-203	15
Hemoglobin (g/L)	6-13	9
Platelet (10×9/L)	9-351	45

AML: Acute myeloid leukemia
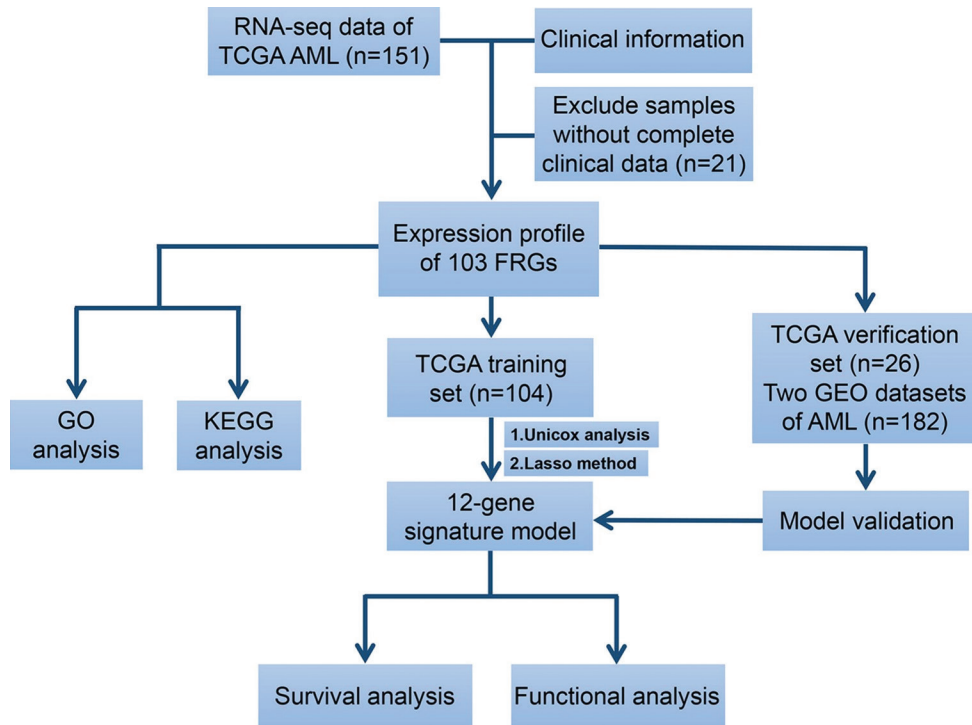
FIGURE 1. Schematic presentation of this study.
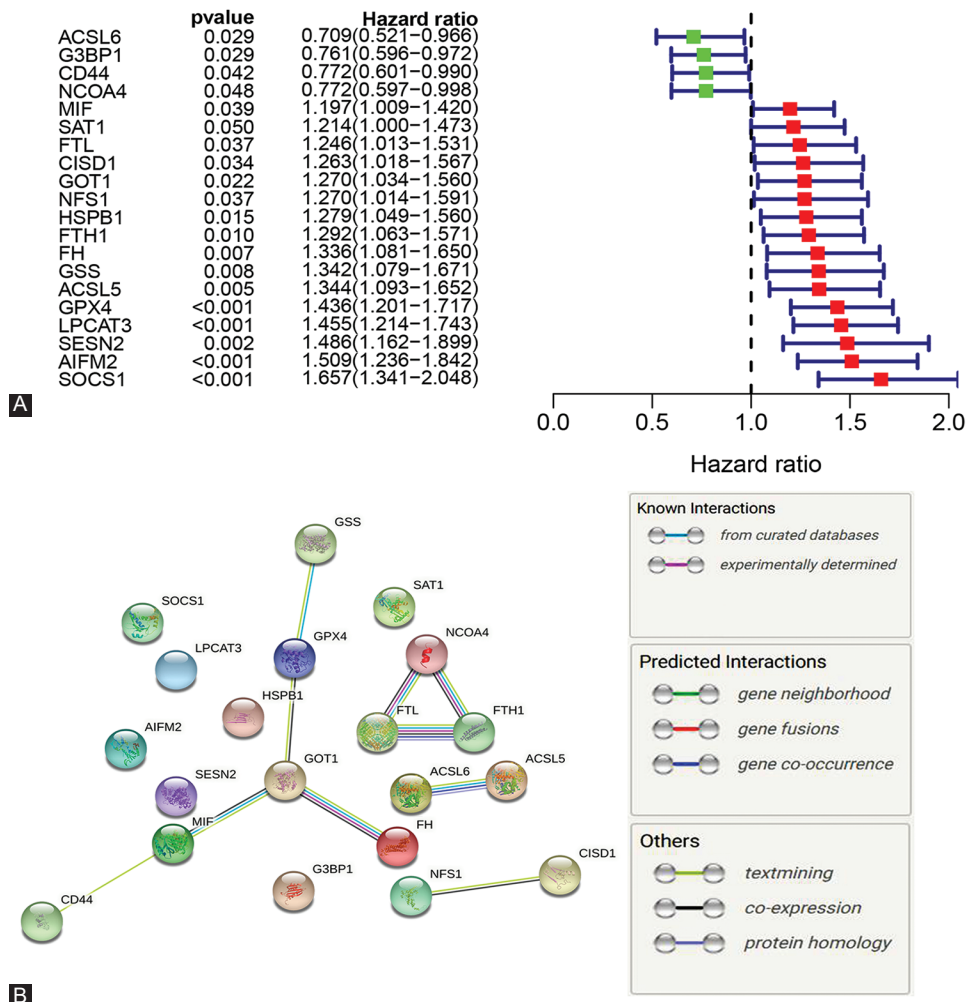
FIGURE 2. Identification of prognostic FRGs in TCGA AML cohort. (A) Forest plot with hazard ratios of the univariate Cox proportional hazards regression analysis between FRGs expression and OS. (B) PPI network for interactions among the 20 FRGs. FRGs: Ferroptosis-related genes, AML: Acute myeloid leukemia, OS: Overall survival.

mitochondria, outer membrane of organelles, and in autophagosomes. In terms of molecular function, these genes were highly enriched in ubiquitin-like protein ligase binding and ubiquitin protein ligase binding (Figure 3A and B). KEGG pathway analysis (Figure 3C and D) revealed that AML-associated FRGs were enriched in various pathways, especially ferroptosis, fatty acid biosynthesis, mineral absorption, adipocytokine signaling pathway, and p53 signaling.

Prognostic gene signatures associated with AML and ferroptosis

To assess the prognostic value of FRGs in AML, the TCGA AML cohort was randomized into verification and training sets at a 1:4 ratio and LASSO Cox regression analysis used to develop a prognostic model based on expression levels of the 20 FRGs, generating a 12-gene signature

(Figure 4A-C and Table S3). Patients' risk scores were evaluated from regression coefficients and expression levels. Risk score signatures were evaluated through the formula: Risk score = (−0.164270341) * acyl-CoA synthetase long-chain family (ACSL)6 levels + (−0.05745754) * Ras-GTPase-activating protein-binding protein 1 (G3BP1) levels + (−0.012600572) * CD44 levels + 0.011883347 * FH levels + 0.040188616 * GPX4 levels + 0.070266332 * CISD1 levels + 0.073905513 * SESN2 levels + 0.074774143 * LPCAT3 levels + 0.075162582 * AIFM2 levels + 0.115640755 * ACSL5 levels + 0.184767081 * HSPB1 levels + 0.287328369 * SOCS1 levels.

To evaluate the signatures' performance, patients were stratified into a low- and high-risk group based on median cut-off values and expressions of the 12 FRGs shown on a heatmap (Figure 4D). Kaplan–Meier analysis revealed that relative to low-risk patient group, in both training set and verification set,
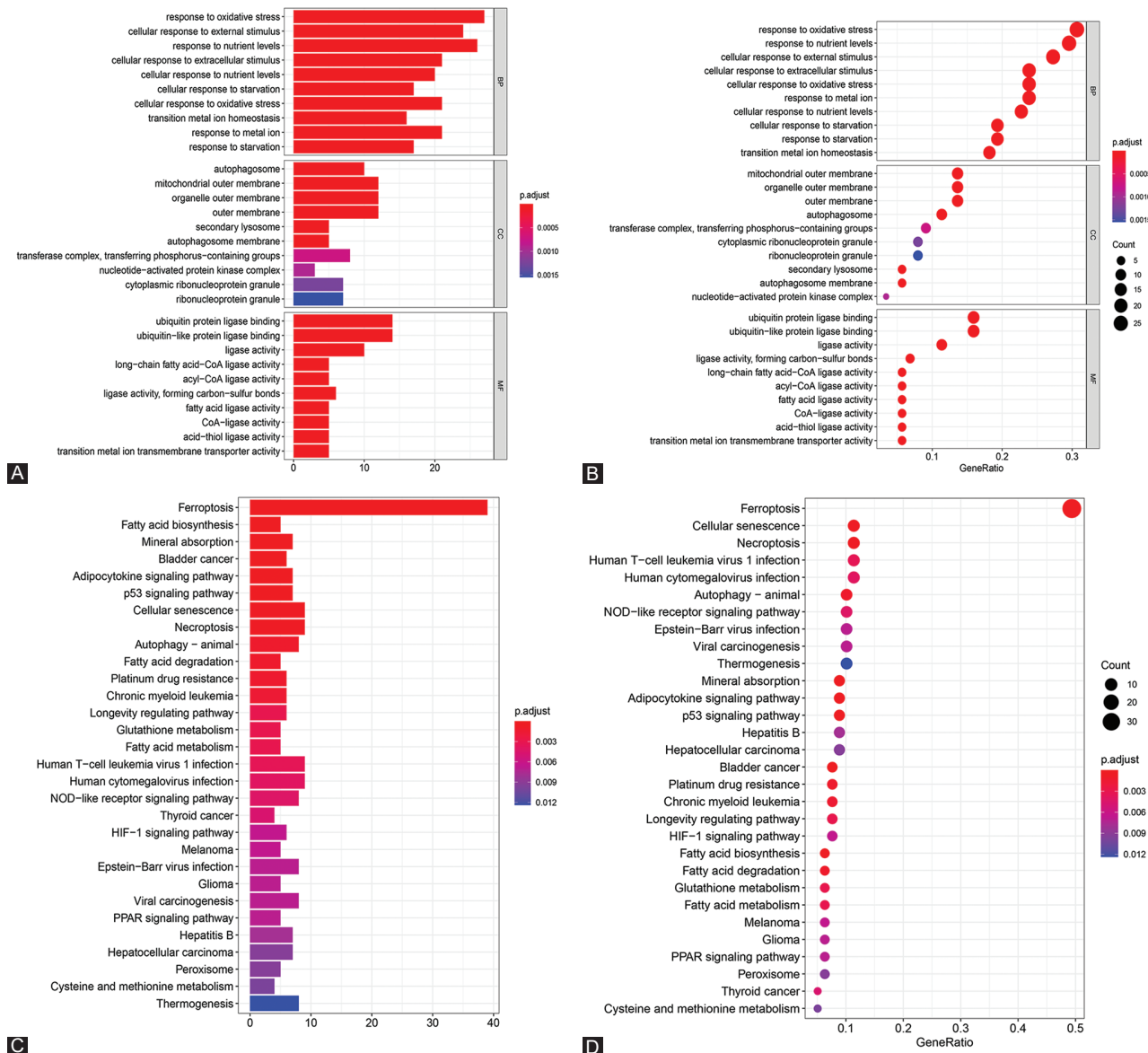
FIGURE 3. GO and KEGG analyses of AML-associated FRGs. (A and B) GO enrichment. (C and D) KEGG pathway enrichment. GO: Gene ontology, KEGG: Kyoto encyclopedia of genes and genomes, FRGs: Ferroptosis-related genes, AML: Acute myeloid leukemia.
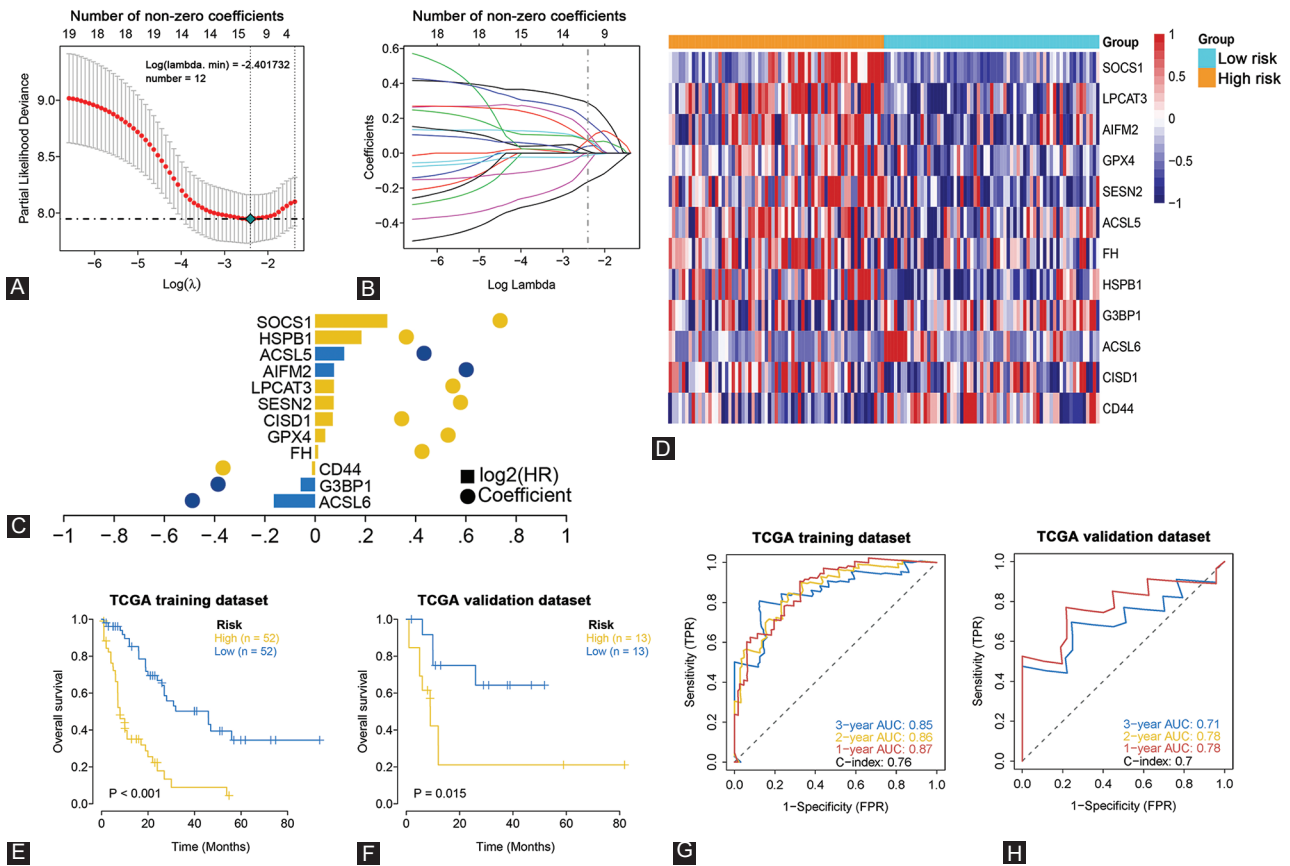
FIGURE 4. Establishment of a 12 FRGs risk signature for OS by LASSO regression analysis in the TCGA cohort. (A) Ten-fold cross-validation for tuning parameter (lambda) selection in the LASSO model. (B) The LASSO coefficient profile plot was created against the log (lambda) sequence. (C) Results of 12 selected FRGs and their regression coefficients by LASSO. (D) Heatmap of the levels of the 12 FRGs in high- and low-risk score groups. (E and F) Kaplan–Meier curve analysis of AML patients' OS stratified by risk score in the TCGA training and validation sets. (G and H) Time-dependent ROC curves in the TCGA training and validation sets. FRGs: Ferroptosis-related genes, OS: Overall survival, LASSO: Least absolute shrinkage and selection operator, ROC: Receiver operating characteristic, AML: Acute myeloid leukemia.

the high-risk AML patient group exhibited markedly worse OS (Figure 4E and F). From ROC curves, risk score signature AUC values of 0.87 (1 year), 0.86 (2 years), and 0.85 (3 years) in the training set as well as a C-index of 0.76 were obtained (Figure 4G). In the validation set, the AUC values were 0.78 for 1 year, 0.78 for 2 years, and 0.71 for 3 years and a C-index of 0.7 (Figure 4H). The results implied that the FRGs signature exhibited a modest AML survival predictive power.

Validation of the 12 FRGs signature on independent cohorts

GEO datasets GSE71014 and GSE12417 were independent cohorts for external validation. AML patients in the GEO dataset were grouped into high- or low-risk patient groups with regard to the median risk score obtained as calculated for the TCGA dataset. Kaplan–Meier analysis results confirmed the signature's prognostic ability, with high-risk patients exhibiting low OS relative to low-risk patient groups in GSE71014 and GSE12417 (Figure 5A and B). In the GSE71014 dataset, AUC values for the risk score signature were 0.72 (1 year), 0.79 (2 years), and 0.75 (3 years), with a C-index of 0.68

(Figure 5C). In GSE12417 dataset, AUC values were 0.68 for 1 year, 0.62 for 2 years, and 0.58 for 3 years with a C-index of 0.61 (Figure 5D). Our data strongly confirmed the 12 FRGs signature's high prognostic capacity for AML.

Functional analysis in high- and low-risk patient groups using GSEA

To establish risk score-associated biological functions and pathways, we subjected differentially expressed genes (DEGs) in high- versus low-risk AML groups in the TCGA cohort to GSEA-based GO and KEGG analysis. GO-GSEA results showed that several biological functions were alternated in patients with high-risk scores, such as glutathione metabolic process and PL catabolic process (Figure 6A). KEGG-GSEA analysis showed that several pathways, including phenylalanine metabolism and pyruvate metabolism, were markedly enriched in the high-risk patient group (Figure 6B). Taken together, these findings indicate that by affecting these cellular processes as well as pathways, DEGs in high-risk groups cause poor AML prognosis.
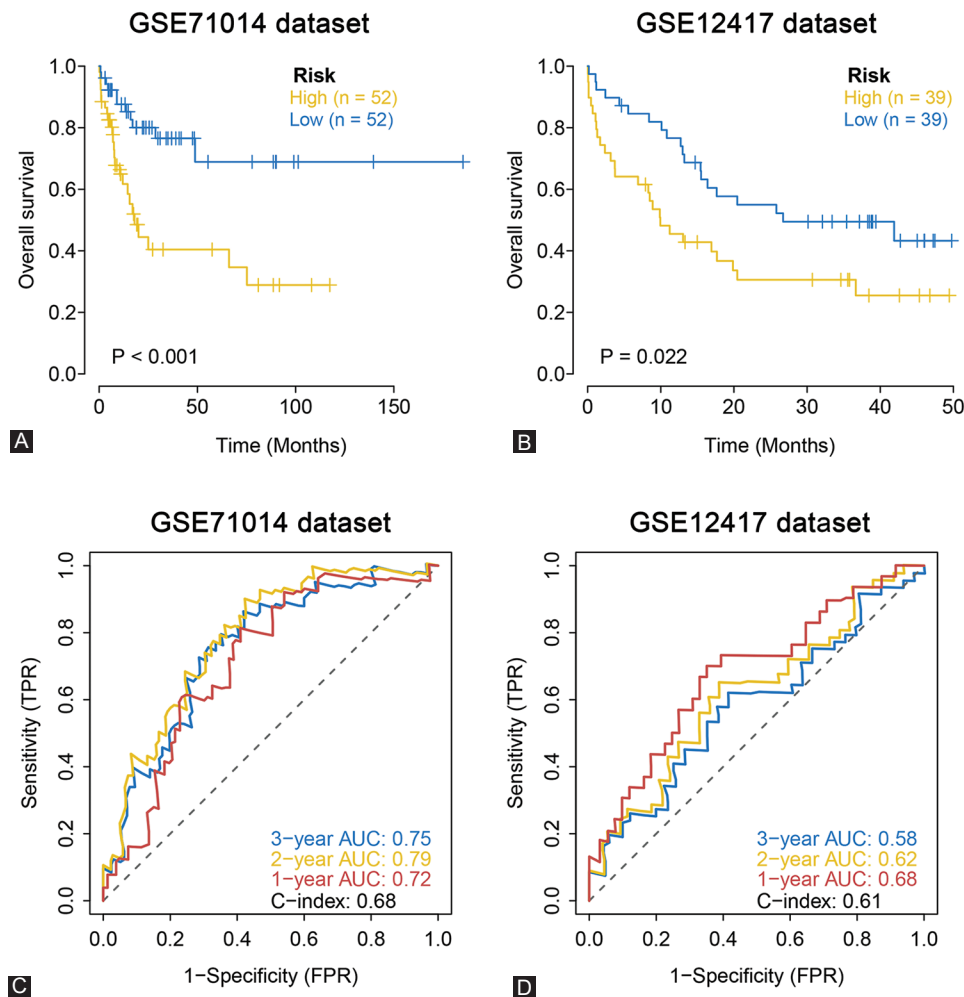
FIGURE 5. External validation of the 12 FRGs signature in the GEO cohort. (A and B) Kaplan–Meier curves for the OS of patients in different risk groups of two GEO external validation datasets. (C and D) AUC of time-dependent ROC curves in the two GEO.

Immune correlations with the 12 FRGs signature

To study the relationships between risk scores and immunity in the TCGA AML cohort, we assessed correlation between immune cell infiltrations and risk scores using CIBERSORT analysis of the distribution of 22 TIICs in high- versus low-risk AML subgroups. This analysis found that compared to low-risk patient groups, the high-risk group contained a markedly higher proportion of M2 macrophages and monocytes, while resting mast cells and gamma-delta T-cells were low (Figure 7A). Based on the 22 immune cells and risk score, we also established an immune infiltration interaction network (Figure 7B). Next, analysis of Spearman correlations of risk scores and levels of immune-related factors in the TISIDB database, such as immune cell receptor-related genes and immune regulatory genes (chemokines and its receptors, immune inhibitory and stimulatory factors, as well as MHC), revealed that levels of cell receptor-associated genes (EIF4A1, SPCS3, GRB2, BCL2, MPZL1, NOL11, CD302, CFLAR, ATP10D, and CDC5L) were generally upregulated (log2 fold change >2.5) in high-risk group (Figure S1A and Table S4). In addition, some immune regulatory genes

showed marked differential expressions (log2 fold change >2.5 or <–2.5) between high- and low-risk groups (B2M, CD96, TAPBP, CD244, TGFBR1, IL2RA, CCR1, HLA-DMA, and HLA-B) (Figure S1B and Table S5). These analyses confirmed that the 12 FRG-based AML risk scores are strongly associated with TIICs infiltration levels and play key roles in tumor immune microenvironment. Correlation assessment of the association between risk score and immune checkpoint-related genes found that PD-L1, LAG3, TGFB1, TNFSF13, CD4, CD40, CD80 (B7-1), and CD276 (B7-H3) positively related to the risk score (Figure 7C). In other words, AML patients with higher risk scores had higher expression levels of these immune checkpoints.

The association between drug sensitivity and the 12 FRGs signature

Based on drug sensitivity data on GDSC, we analyzed the correlation between the 12 FRGs risk score with IC_{50} of some chemotherapy or targeted drugs used against hematological malignancies. We presumed that a positive correlation between risk score and IC_{50} value would indicate a basis for

GO-GSEA

KEGG-GSEA
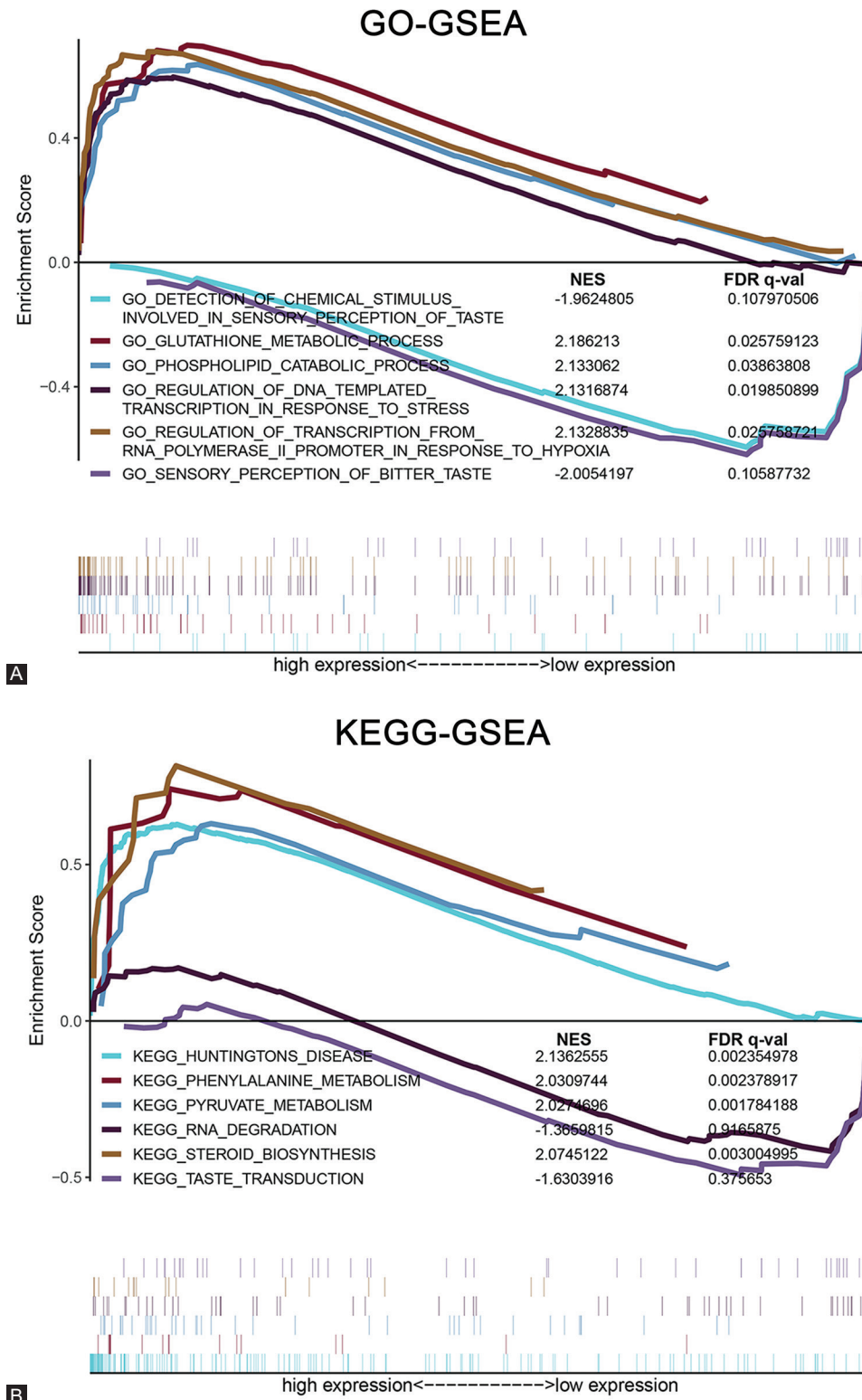
FIGURE 6. GSEA analysis of DEGs between low- and high-risk AML subgroups. (A) GSEA GO term enrichment. (B) GSEA KEGG pathway enrichment. GSEA: Gene set enrichment analysis, DEGs: Differentially expressed genes, AML: Acute myeloid leukemia, GO: Gene ontology, KEGG: Kyoto encyclopedia of genes and genomes.

developing drug resistance in high-risk group patients, while a negative association implies a higher drug sensitivity in these patients. This analysis showed that AML patients in high-risk group had a worse response (higher IC_{50}) to Midostaurin, ABT-263, Bleomycin, Bosutinib and Lenalidomide ($p <$ 0.05; Figure 8A-E) and were more sensitive (lower IC_{50}) to Vinblastine, Dasatinib, Gemcitabine, Etoposide, and Obatoclax mesylate ($p < 0.05$; Figure 8F-J).
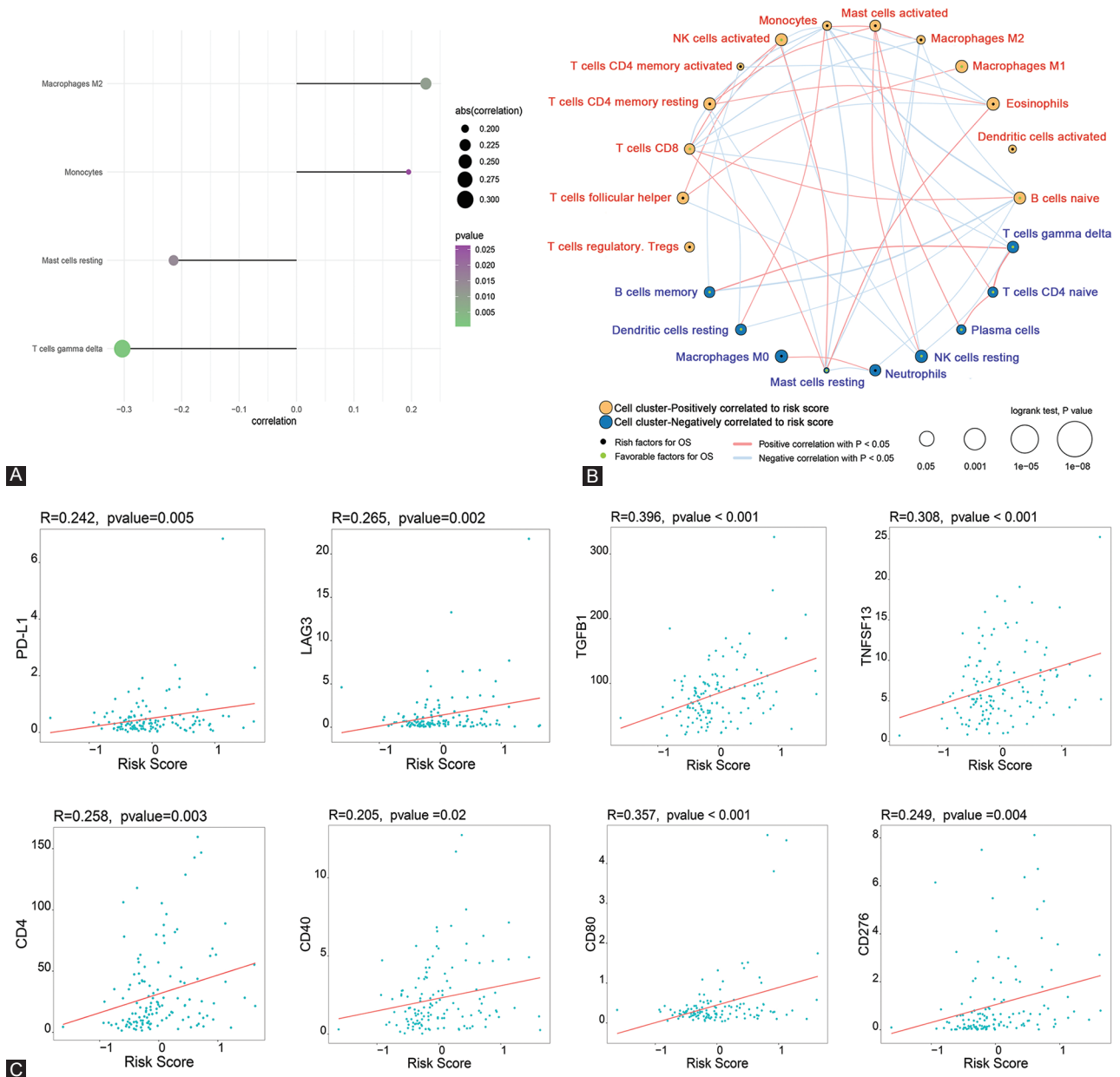
FIGURE 7. Association between immune status and the 12 FRGs signature. (A) Immune cell component comparisons between low- and high-risk AML subgroups by CIBERSORT. (B) Immune cell infiltration interaction network based on the risk scores and the 22 immune cells. (C) Correlation analysis of the expressions of eight immune checkpoints with 12 FRGs based risk scores. FRGs: Ferroptosis-related genes, AML: Acute myeloid leukemia.

DISCUSSION

According to the latest statistics, 5-year AML survival from 2010 to 2016 is <30% [30]. Most AML patients experience relapse or primary refractory disease, which are hard to treat [4]. Cancer resistance to apoptosis is a major obstacle to successful treatment, resulting in many cancer-associated deaths [31]. Resistance to apoptosis is also a significant hallmark in relapsed/refractory AML [6,7]. Thus, treatments that induce non-apoptotic cell death may improve AML outcomes.

Ferroptosis, a novel form of RCD, is defined by unique morphology, genetics, as well as biochemistry. Since ferroptosis mechanisms differ from apoptosis, it can overcome the low

efficacies of apoptosis-initiating drugs. Ferroptosis is mainly induced by iron-dependent enhancement of lipid peroxidation to lethal levels. Several small molecules promote ferroptosis, including erastin and RSL3 [13], and some novel agents can trigger ferroptosis in AML cells [17-21]. These ferroptosis inducers offer alternatives for apoptosis-resistant cases [32]. Ferroptosis is a complex process regulated by various genes [33]. However, the molecular basis of ferroptosis in cancer, including AML, needs further study. Hence, identification of FRG signatures in AML will elucidate on ferroptosis regulatory networks and inform biomarker-based risk stratifications for ferroptosis-associated therapy. Here, we assessed the levels of 103 FRGs in AML patients and their correlation with
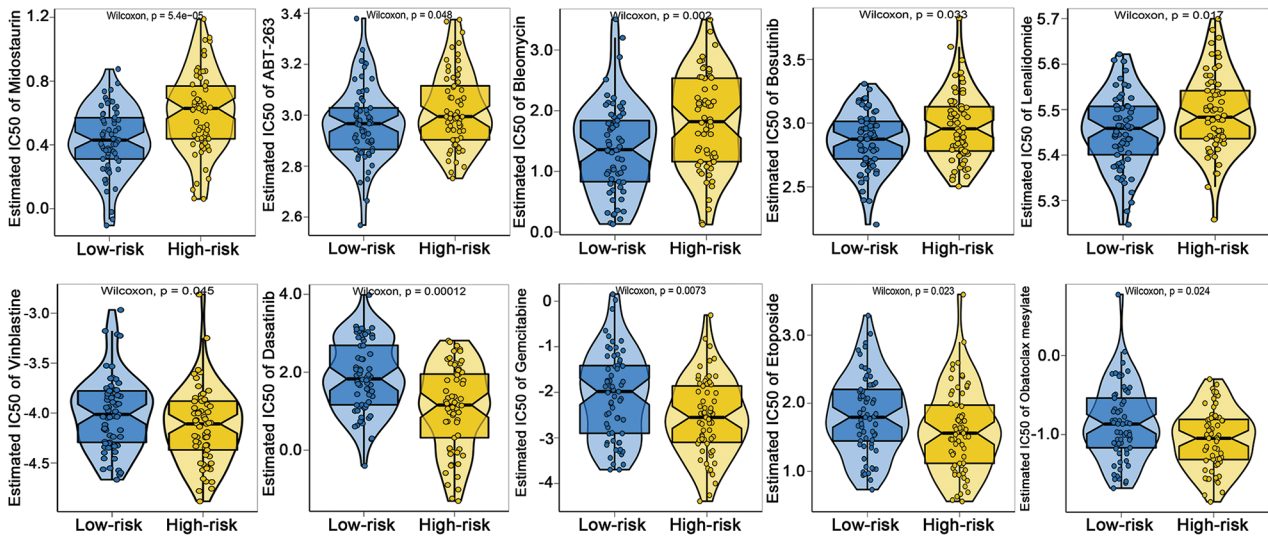
FIGURE 8. (A-J) Association between risk-related FRGs and drug resistance. Plots denote correlation of risk scores with the IC_{50} of various drugs on AML patients. FRGs: Ferroptosis-related genes, AML: Acute myeloid leukemia.

prognosis. First, a new 12 FRGs prognostic signature was constructed and validated on internal and external cohorts. Based on this model, our functional analyses revealed differential pathways and biological functions between high- and low-risk subgroups, as well as differences in the immune microenvironment and treatment sensitivity.

Using publicly available AML datasets, we for the 1st time show that FRGs can classify patients into high- and low-risk patient subgroups that exhibit marked differences in clinical prognosis and biological features. LASSO regression analysis was used to develop a 12 FRG-based prognostic risk model comprised 10 risk-related genes (GPX4, CD44, FH, CISD1, SESN2, LPCAT3, AIFM2, ACSL5, HSPB1, and SOCS1) and two protective genes (ACSL6 and G3BP1). Thus, AML patients can be classified into subgroups with different risk scores to predict clinical outcomes. Based on function, the 12 FRGs can be grouped into four classes: Lipid metabolism (GPX4, LPCAT3, ACSL5, and ACSL6), antioxidant metabolism (CD44, SESN2, and AIFM2), iron metabolism (CISD1 and HSPB1), and cancer metabolism (SOCS1, FH, and G3BP1) [14,33-36]. GPX4, a central negative regulator of ferroptosis, functions as a lipid repair enzyme that suppresses PL hydroperoxide levels within membranes as well as lipoproteins, inhibiting ferroptosis induction. GPX4 inactivation or degradation induces rapid lipid peroxides accumulation, contributing to ferroptosis [11,12]. GPX4 is elevated in various cancer types where it enhances anti-cancer drug resistance [37]. GPX4 overexpression in AML correlates with poor prognosis [15]. LPCAT3 catalyzes the insertion of arachidonic acid into polyunsaturated fatty acid-containing PLs and can make cells resistant to ferroptosis [38]. LPCAT3 is reported to regulate intestinal stem cell proliferation and enhance tumor formation [39]. ACSL5 and ACSL6 belong to the ACSLs that catalyze activations of

long-chain fatty acids. ACSLs deregulation is reported to promote cancer cell proliferation [36] and the activity of ACSL5 and ACSL6 is often enhanced in some solid tumors like colorectal cancer [36]. On the contrary, ACSL6 downregulation significantly correlates with poor patient survival and acts as a tumor suppressor in AML, which is consistent with our findings [40]. Nevertheless, due to a lack of experimental proof, the functional value of ACSL5 and ACSL6 in ferroptosis remains unclear. For antioxidant metabolism, overexpression of the cancer stem cell marker CD44 enhances the stability of SLC7A11, a key regulator of lipid peroxidation, and inhibits ferroptosis in cancer cells [14]. Notably, CD44 is leukemogenic and correlates with poor AML prognosis [41]. SESN2 is a conserved antioxidant that responds to various stresses, including oxidative stress to restore homeostatic balance. SESN2 is reported to protect against iron overload and ferroptosis in liver injury [35]. In the mitochondria, AIFM2 is regarded as a traditional initiator of apoptosis and has been established to be an antioxidant regulator in ferroptosis, independently of mitochondrial function [33]. SESN2 and AIFM2 are responsible for tumor cell survival [33,35], but their exact functions in AML cells ferroptosis remains uncharacterized. Low iron utilization levels can enhance ferroptosis sensitivity. CISD1 may suppress ferroptosis by inhibiting iron uptake by mitochondria [33] and CISD1 inhibition by small molecular ligand NL-1, which is reported to overcome drug resistance and exert anti-leukemic activity in B-cell acute lymphoblastic leukemia [42]. In various cancer cell types, HSPB1, a heat shock protein, is highly induced by erastin therapy. HSPB1 negatively regulates ferroptosis by inhibiting iron uptake [43]. In terms of cancer metabolism, TP53 gene, a well-known tumor suppressor [44], is inactivated or mutated in most human tumors, such as AML. G3BP1 is a TP53 regulator. Interaction between

G3BP1 and lncRNA P53RRA traps TP53 in the nucleus, leading to TP53-mediated cell cycle arrest, ferroptosis, as well as apoptosis [45]. It is reported that low G3BP1 expression is related to poor AML survival, highlighting the protective role of G3BP1 [46]. Another TP53 regulator, SOCS1, is required for p53 activation and the regulation of cellular senescence and modulates p53 target genes expression (e.g., SLC7A11) and sensitizes cells to ferroptosis [47]. Interestingly, AML patients with elevated SOCS1 levels have been reported to have low complete remission rates and short OS, indicating that SOCS1 is a poor prognosis predictor of AML [48]. Fumarate hydratase (FH), a TCA cycle enzyme, has been shown to be a tumor suppressor and FH loss of function confers cancer cells resistance to ferroptosis. However, FH expression is often upregulated in tumor cells, including renal cancer and AML cells, which can be explained as FH mutation and dysfunction and needs further investigation [34,49]. The 12 FRGs are highly correlated with tumor prognosis and ferroptosis, which provides a vital theoretical basis for our ferroptosis-based AML risk model. Using GSEA-based GO and KEGG analysis, we identified various BP as enriched in the high-risk group, most of which are ferroptosis related, including glutathione (GSH) metabolic process and PL catabolic process [33].

The notion that immunity promotes or suppresses tumorigenesis is well-accepted. During the development of various cancers, immunosuppressive mechanisms are initiated to avoid anti-tumor immune responses. With increasing immunosuppression, low immunogenic cancer cells are selected, resulting in immune escape [50]. Even though the mechanisms involved in tumor predisposition to ferroptosis are a hot topic in recent years, potential modulation between tumor immunity and ferroptosis remains incompletely understood. Based on the 12 FRGs signature, we performed multiple analyses between different AML risk subgroups and discovered that ferroptosis may be highly associated with tumor immunity. In this study, AML patients with higher risk scores identified by the 12 FRGs signature exhibited higher fractions of M2 macrophages and monocytes. Increased infraction by tumor-associated M2 macrophages and monocytes represents a significant predictor of poor clinical AML outcomes [51]. Moreover, the 12 FRGs based risk score had significant positive correlation with most immune inhibitors (including CD96, CD244, and TGFBR1) and showed significant negative correlation with the immune stimulator IL2RA. These results indicated that ferroptosis and iron metabolism regulate the tumor immune microenvironment and that the poor prognostic outcomes in the high-risk patient subgroup may be as a result of stronger immunosuppression. Immune checkpoint manipulation has recently become a vital, effective immunotherapeutic form [52]. Higher expression of PD-L1, LAG3, TGFB1, TNFSF13, CD4, CD40, CD80, and CD276 was found in the high-risk group, which may enhance AML development and progression, leading to poor prognostic outcomes. Our findings imply that the FRGs risk model may be beneficial to the precision immunotherapy of AML patients in the future, especially those of high-risk groups.

Finally, we explored the association between FRGs base risk scores and drug sensitivities in AML patients. AML patients with higher risk scores were predicted to exert a worse sensitivity against anti-tumor agents including Midostaurin (an FLT3 inhibitor), ABT-263 (a BCL-2 inhibitor), Bleomycin, Bosutinib, and Lenalidomide. Interestingly, those patients seem to be more sensitive to another BCL-2 inhibitor, Obatoclax mesylate, which was demonstrated to show only modest efficacy in the treatment of hematological malignancies including AML, and have not been approved for clinical use yet [53]. Our results also suggested that higher risk patients had a better response to Vinblastine, Dasatinib, Gemcitabine, and Etoposide. Although some of these drugs above are not in clinical use of AML treatment or under investigation, elucidation of the association between the 12 FGRs risk model and drug sensitivity may reveal therapeutic markers for further validation. Through molecular stratification of patients, drug sensitivity data can also optimize clinical trial designs for future successful anti-cancer treatments.

Some limitations of this study are also acknowledged. First, our risk model was constructed and validated using existing public datasets and more prospective data are needed to validate its clinical application. Second, the use of a single hallmark (ferroptosis) for prognostic model construction has some intrinsic weakness. This is because various prognostic genes for AML could have been excluded. In addition, our findings need further confirmation in larger experimental and clinical studies.

CONCLUSION

We established a novel prognostic model of 12 FRGs in AML. The model successfully divided patients into high- and low-risk patient groups with mean OS as the basis. The underlying mechanisms between 12 FRGs based risk scores and tumor immunity or drug sensitivity in AML were also discussed. We believe that the 12 FRGs have the potential to become a prognostic biomarker that will offer novel insight into AML research and treatment.

REFERENCES

[1]   Siegel RL, Miller KD, Fuchs HE, Jemal A. Cancer Statistics, 2021. CA Cancer J Clin 2021;71(1):7-33.
      https://doi.org/10.3322/caac.21654
[2]   Short NJ, Rytting ME, Cortes JE. Acute myeloid leukaemia. Lancet 2018; 392:593-606.

https://doi.org/10.1016/S0140-6736(18)31041-9

[3] Döhner H, Weisdorf DJ, Bloomfield CD. Acute myeloid leukemia. N Engl J Med 2015;373(12):1136-52.
https://doi.org/10.1056/NEJMra1406184

[4] Thol F, Schlenk RF, Heuser M, Ganser A. How I treat refractory and early relapsed acute myeloid leukemia. Blood 2015;126(3):319-27.
https://doi.org/10.1182/blood-2014-10-551911

[5] Cassier PA, Castets M, Belhabri A, Vey N. Targeting apoptosis in acute myeloid leukaemia. Br J Cancer 2017;117(8):1089-98.
https://doi.org/10.1038/bjc.2017.281

[6] Reyna DE, Garner TP, Lopez A, Kopp F, Choudhary GS, Sridharan A, et al. Direct activation of BAX by BTSA1 overcomes apoptosis resistance in acute myeloid leukemia. Cancer Cell 2017;32(4):490-505.e10.
https://doi.org/10.1016/j.ccell.2017.09.001

[7] Fulda S, Debatin KM. Extrinsic versus intrinsic apoptosis pathways in anticancer chemotherapy. Oncogene 2006;25(34):4798-811.
https://doi.org/10.1038/sj.onc.1209608

[8] Yan HF, Zou T, Tuo QZ, Xu S, Li H, Belaidi AA, et al. Ferroptosis: Mechanisms and links with diseases. Signal Transduct Target Ther 2021;6(1):49.
https://doi.org/10.1038/s41392-020-00428-9

[9] Dixon SJ, Lemberg KM, Lamprecht MR, Skouta R, Zaitsev EM, Gleason CE, et al. Ferroptosis: An iron-dependent form of nonapoptotic cell death. Cell 2012;149(5):1060-72.
https://doi.org/10.1016/j.cell.2012.03.042

[10] Angeli JP, Schneider M, Proneth B, Tyurina YY, Tyurin VA, Hammond VJ, et al. Inactivation of the ferroptosis regulator Gpx4 triggers acute renal failure in mice. Nat Cell Biol 2014;16(12):1180-91.
https://doi.org/10.1038/ncb3064

[11] Yang WS, SriRamaratnam R, Welsch ME, Shimada K, Skouta R, Viswanathan VS, et al. Regulation of ferroptotic cancer cell death by GPX4. Cell 2014;156(1-2):317-31.
https://doi.org/10.1016/j.cell.2013.12.010

[12] Stockwell BR, Angeli JP, Bayir H, Bush AI, Conrad M, Dixon SJ, et al. Ferroptosis: A regulated cell death nexus linking metabolism, redox biology, and disease. Cell 2017;171(2):273-85.
https://doi.org/10.1016/j.cell.2017.09.021

[13] Liang C, Zhang X, Yang M, Dong X. Recent progress in ferroptosis inducers for cancer therapy. Adv Mater 2019;31(51):e1904197.
https://doi.org/10.1002/adma.201904197

[14] Hassannia B, Vandenabeele P, Vanden Berghe T. Targeting ferroptosis to iron out cancer. Cancer Cell 2019;35(6):830-49.
https://doi.org/10.1016/j.ccell.2019.04.002

[15] Wei J, Xie Q, Liu X, Wan C, Wu W, Fang K, et al. Identification the prognostic value of glutathione peroxidases expression levels in acute myeloid leukemia. Ann Transl Med 2020;8(11):678.
https://doi.org/10.21037/atm-20-3296

[16] Yusuf RZ, Saez B, Sharda A, van Gastel N, Yu VW, Baryawno N, et al. Aldehyde dehydrogenase 3a2 protects AML cells from oxidative death and the synthetic lethality of ferroptosis inducers. Blood 2020;136(11):1303-16.
https://doi.org/10.1182/blood.2019001808

[17] Birsen R, Larrue C, Decroocq J, Johnson N, Guiraud N, Gotanegre M, et al. APR-246 induces early cell death by ferroptosis in acute myeloid leukemia. Haematologica 2021; Online ahead of print.
https://doi.org/10.3324/haematol.2020.259531

[18] Du Y, Bao J, Zhang MJ, Li LL, Xu XL, Chen H, et al. Targeting ferroptosis contributes to ATPR-induced AML differentiation via ROS-autophagy-lysosomal pathway. Gene 2020;755:144889.
https://doi.org/10.1016/j.gene.2020.144889

[19] Young MM, Bui V, Chen C, Wang HG. FTY720 induces non-canonical phosphatidylserine externalization and cell death in acute myeloid leukemia. Cell Death Dis 2019;10(11):847.
https://doi.org/10.1038/s41419-019-2080-5

[20] Zhu HY, Huang ZX, Chen GQ, Sheng F, Zheng YS. Typhaneoside prevents acute myeloid leukemia (AML) through suppressing proliferation and inducing ferroptosis associated with autophagy. Biochem Biophys Res Commun 2019;516(4):1265-71.
https://doi.org/10.1016/j.bbrc.2019.06.070

[21] Du J, Wang T, Li Y, Zhou Y, Wang X, Yu X, et al. DHA inhibits proliferation and induces ferroptosis of leukemia cells through autophagy dependent degradation of ferritin. Free Radic Biol Med 2019;131:356-69.
https://doi.org/10.1016/j.freeradbiomed.2018.12.011

[22] Yu G, Wang LG, Han Y, He QY. clusterProfiler: An R package for comparing biological themes among gene clusters. OMICS 2012;16(5):284-7.
https://doi.org/10.1089/omi.2011.0118

[23] Tibshirani R. The lasso method for variable selection in the Cox model. Stat Med 1997;16(4):385-95.
https://doi.org/10.1002/(sici) 1097-0258 (19970228) 16:4<385: aid-sim380>3.0.co;2-3

[24] Geeleher P, Cox NJ, Huang RS. pRRophetic: An R package for prediction of clinical chemotherapeutic response from tumor gene expression levels. PLoS One 2014;9(9):e107468.
https://doi.org/10.1371/journal.pone.0107468

[25] Geeleher P, Cox NJ, Huang RS. Clinical drug response can be predicted using baseline gene expression levels and *in vitro* drug sensitivity in cell lines. Genome Biol 2014;15(3):R47.
https://doi.org/10.1186/gb-2014-15-3-r47

[26] Newman AM, Liu CL, Green MR, Gentles AJ, Feng W, Xu Y, et al. Robust enumeration of cell subsets from tissue expression profiles. Nat Methods 2015;12(5):453-7.
https://doi.org/10.1038/nmeth.3337

[27] Subramanian A, Tamayo P, Mootha VK, Mukherjee S, Ebert BL, Gillette MA, et al. Gene set enrichment analysis: A knowledge-based approach for interpreting genome-wide expression profiles. Proc Natl Acad Sci USA 2005;102(43):15545-50.
https://doi.org/10.1073/pnas.0506580102

[28] Liberzon A, Subramanian A, Pinchback R, Thorvaldsdóttir H, Tamayo P, Mesirov JP. Molecular signatures database (MSigDB) 3.0. Bioinformatics 2011;27(12):1739-40.
https://doi.org/10.1093/bioinformatics/btr260

[29] Ru B, Wong CN, Tong Y, Zhong JY, Zhong SS, Wu WC, et al. TISIDB: An integrated repository portal for tumor-immune system interactions. Bioinformatics 2019;35(20):4200-2.
https://doi.org/10.1093/bioinformatics/btz210

[30] National Cancer Institute. Cancer Stat Facts: Leukemia-Acute Myeloid Leukemia (AML);2021. Available from: https://www.seer.cancer.gov/statfacts/html/amyl.html. Accessed July 1st, 2021.

[31] Housman G, Byler S, Heerboth S, Lapinska K, Longacre M, Snyder N, et al. Drug resistance in cancer: An overview. Cancers (Basel) 2014;6(3):1769-92.
https://doi.org/10.3390/cancers6031769

[32] Shen Z, Song J, Yung BC, Zhou Z, Wu A, Chen X. Emerging strategies of cancer therapy based on ferroptosis. Adv Mater 2018;30(12):e1704007.
https://doi.org/10.1002/adma.201704007

[33] Tang D, Chen X, Kang R, Kroemer G. Ferroptosis: Molecular mechanisms and health implications. Cell Res 2021;31(2):107-25.
https://doi.org/10.1038/s41422-020-00441-1

[34] Gao M, Yi J, Zhu J, Minikes AM, Monian P, Thompson CB, et al. Role of mitochondria in ferroptosis. Mol Cell 2019;73(2):354-63.e3.
https://doi.org/10.1016/j.molcel.2018.10.042

[35] Park SJ, Cho SS, Kim KM, Yang JH, Kim JH, Jeong EH, et al. Protective effect of sestrin2 against iron overload and ferroptosis-induced liver injury. Toxicol Appl Pharmacol 2019;379:114665.
https://doi.org/10.1016/j.taap.2019.114665

[36] Rossi Sebastiano M, Konstantinidou G. Targeting long chain acyl-CoA synthetases for cancer therapy. Int J Mol Sci 2019;20(15):3624.
https://doi.org/10.3390/ijms20153624

[37] Yang L, Chen X, Yang Q, Chen J, Huang Q, Yao L, et al. Broad spectrum deubiquitinase inhibition induces both apoptosis and ferroptosis in cancer cells. Front Oncol 2020;10:949.
https://doi.org/10.3389/fonc.2020.00949

[38] Kagan VE, Mao G, Qu F, Angeli JP, Doll S, Croix CS, et al. Oxidized arachidonic and adrenic PEs navigate cells to ferroptosis. Nat Chem Biol 2017;13(1):81-90.

https://doi.org/10.1038/nchembio.2238

[39] Wang B, Rong X, Palladino EN, Wang J, Fogelman AM, Martin MG, et al. Phospholipid remodeling and cholesterol availability regulate intestinal stemness and tumorigenesis. Cell Stem Cell 2018;22(2):206-20.e4.
https://doi.org/10.1016/j.stem.2017.12.017

[40] Chen WC, Wang CY, Hung YH, Weng TY, Yen MC, Lai MD. Systematic Analysis of gene expression alterations and clinical outcomes for long-chain acyl-coenzyme a synthetase family in cancer. PLoS One 2016;11:e0155660.
https://doi.org/10.1371/journal.pone.0155660

[41] Gutjahr JC, Bayer E, Yu X, Laufer JM, Höpner JP, Tesanovic S, et al. CD44 engagement enhances acute myeloid leukemia cell adhesion to the bone marrow microenvironment by increasing VLA-4 avidity. Haematologica 2020;106(8):2102-13.
https://doi.org/10.3324/haematol.2019.231944

[42] Geldenhuys WJ, Nair RR, Piktel D, Martin KH, Gibson LF. The MitoNEET ligand NL-1 mediates antileukemic activity in drug-resistant B-cell acute lymphoblastic leukemia. J Pharmacol Exp Ther 2019;370(1):25-34.
https://doi.org/10.1124/jpet.118.255984

[43] Sun X, Ou Z, Xie M, Kang R, Fan Y, Niu X, et al. HSPB1 as a novel regulator of ferroptotic cancer cell death. Oncogene 2015;34(45):5617-25.
https://doi.org/10.1038/onc.2015.32

[44] Kaiser AM, Attardi LD. Deconstructing networks of p53-mediated tumor suppression *in vivo*. Cell Death Differ 2018;25(1):93-103.
https://doi.org/10.1038/cdd.2017.171

[45] Mao C, Wang X, Liu Y, Wang M, Yan B, Jiang Y, et al. A G3BP1-Interacting lncRNA promotes ferroptosis and apoptosis in cancer via nuclear sequestration of p53. Cancer Res 2018;78(13):3484-96.
https://doi.org/10.1158/0008-5472.CAN-17-3454

[46] Goldgraben MA, Fewings E, Larionov A, Scarth J, Redman J, Telford N, et al. Genomic profiling of acute myeloid leukaemia associated with ataxia telangiectasia identifies a complex karyotype with wild-type TP53 and mutant KRAS, G3BP1 and IL7R. Pediatr Blood Cancer 2020;67(9):e28354.
https://doi.org/10.1002/pbc.28354

[47] Saint-Germain E, Mignacca L, Vernier M, Bobbala D, Ilangumaran S, Ferbeyre G. SOCS1 regulates senescence and ferroptosis by modulating the expression of p53 target genes. Aging (Albany NY) 2017;9(10):2137-62.
https://doi.org/10.18632/aging.101306

[48] Hou HA, Lu JW, Lin TY, Tsai CH, Chou WC, Lin CC, et al. Clinicobiological significance of suppressor of cytokine signaling 1 expression in acute myeloid leukemia. Blood Cancer J 2017;7(7):e588.
https://doi.org/10.1038/bcj.2017.67

[49] Elo LL, Karjalainen R, Ohman T, Hintsanen P, Nyman TA, Heckman CA, et al. Statistical detection of quantitative protein biomarkers provides insights into signaling networks deregulated in acute myeloid leukemia. Proteomics 2014;14(21-22):2443-53.
https://doi.org/10.1002/pmic.201300460

[50] Dunn GP, Bruce AT, Ikeda H, Old LJ, Schreiber RD. Cancer immunoediting: From immunosurveillance to tumor escape. Nat Immunol 2002;3(11):991-8.
https://doi.org/10.1038/ni1102-991

[51] Xu ZJ, Gu Y, Wang CZ, Jin Y, Wen XM, Ma JC, et al. The M2 macrophage marker CD206: A novel prognostic indicator for acute myeloid leukemia. Oncoimmunology 2019;9(1):1683347.
https://doi.org/10.1080/2162402X.2019.1683347

[52] Abril-Rodriguez G, Ribas A. SnapShot: Immune checkpoint inhibitors. Cancer Cell 2017;31(6):848-848.e1.
https://doi.org/10.1016/j.ccell.2017.05.010

[53] Goard CA, Schimmer AD. An evidence-based review of obatoclax mesylate in the treatment of hematological malignancies. Core Evid 2013;8:15-26.
https://doi.org/10.2147/CE.S42568

Related articles published in BJBMS

1. Development and validation of a ferroptosis-related lncRNAs prognosis signature in colon cancer
Hua-jun Cai et al., BJBMS, 2021

2. The prognostic significance of different proportion of signet-ring cells of colorectal carcinoma
Wei Chen et al., BJBMS, 2020

SUPPLEMENTAL DATA
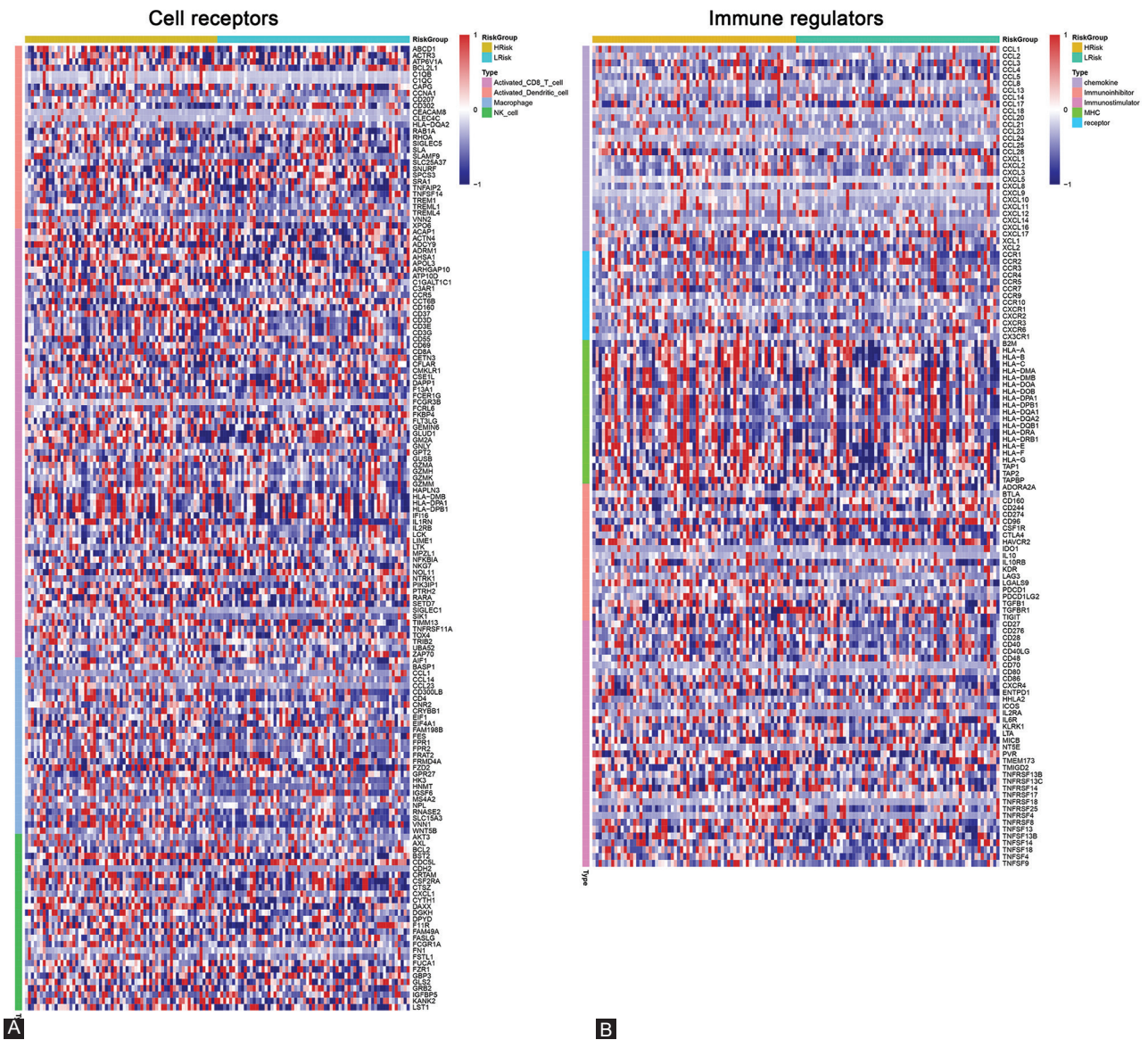
FIGURE S1. (A and B) Heatmaps of correlation between immune factors and 12 FRGs by the TISIDB database. FRGs: Ferroptosis-related genes.

TABLE S1. List of the 94 FRGs enrolled in this study

Gene symbol	Description
ACSL1	Acyl-CoA synthetase long-chain family member 1
ACSL3	Acyl-CoA synthetase long-chain family member 3
ACSL4	Acyl-CoA synthetase long-chain family member 4
ACSL5	Acyl-CoA synthetase long-chain family member 5
ACSL6	Acyl-CoA synthetase long-chain family member 6
AIFM2	Apoptosis inducing factor mitochondria associated 2
ALOX12	Arachidonate 12-Lipoxygenase, 12S Type
ALOX15B	Arachidonate 15-Lipoxygenase Type B
ANO6	Anoctamin 6
ARNTL	Aryl hydrocarbon receptor nuclear translocator like
ATF4	Activating transcription factor 4
ATG5	Autophagy related 5
ATG7	Autophagy related 7
AURKA	Aurora kinase A
BAP1	BRCA1-associated protein 1
BECN1	Beclin 1
CASP8	Caspase 8
CD44	CD44 molecule (Indian Blood Group)
CDKN2A	Cyclin-dependent kinase inhibitor 2A
CFTR	CF transmembrane conductance regulator
CISD1	CDGSH iron sulfur domain 1
CP	Ceruloplasmin
CYBB	Cytochrome B-245 beta chain
EGLN1	Egl-9 family hypoxia-inducible factor 1
ELAVL1	ELAV-like RNA-binding protein 1
EPAS1	Endothelial PAS domain protein 1
FANCD2	FA complementation Group D2
FH	Fumarate hydratase
FTH1	Ferritin heavy chain 1
FTL	Ferritin light chain
G3BP1	G3BP stress granule assembly factor 1
GCLC	Glutamate-cysteine ligase catalytic subunit
GCLM	Glutamate-cysteine ligase modifier subunit
GOT1	Glutamic-oxaloacetic transaminase 1
GPX4	Glutathione peroxidase 4
GSS	Glutathione synthetase
GUCY1A1	Guanylate cyclase 1 soluble subunit alpha 1
HELLS	Helicase, lymphoid specific
HILPDA	Hypoxia-inducible lipid droplet associated
HMGB1	High mobility group box 1
HMOX1	Heme oxygenase 1
HSPA5	Heat shock protein family A (Hsp70) member 5
HSPB1	Heat shock protein family B (Small) member 1
ITGA6	Integrin subunit alpha 6
LAMP2	Lysosomal-associated membrane protein 2
LINC00336	Long intergenic non-protein coding RNA 336
LINC00472	Long intergenic non-protein coding RNA 472
LPCAT3	Lysophosphatidylcholine acyltransferase 3
MAP1LC3A	Microtubule-associated protein 1 light chain 3 alpha
MAP1LC3B	Microtubule-associated protein 1 light chain 3 beta
MAP1LC3B2	Microtubule-associated protein 1 light chain 3 beta 2
MAP1LC3C	Microtubule-associated protein 1 light chain 3 gamma
MAP3K5	Mitogen-activated protein 3 kinase 5
MAPK1	Mitogen-activated protein kinase 1
MDM2	MDM2 proto-oncogene
MIF	Macrophage migration inhibitory factor
MT1G	Metallothionein 1G
MUC1	Mucin 1, cell surface associated
MYC	MYC proto-oncogene, BHLH transcription factor

(Contd....)

TABLE S1. *(Continued)*

Gene symbol	Description
NCOA4	Nuclear receptor coactivator 4
NEDD4	NEDD4 E3 ubiquitin protein ligase
NF2	Neurofibromin 2
NFE2L2	Nuclear factor, erythroid 2 like 2
NFS1	NFS1 cysteine desulfurase
NGB	Neuroglobin
OTUB1	OTU deubiquitinase, ubiquitin aldehyde binding 1
PCBP1	Poly (RC)-binding protein 1
PCBP2	Poly (RC)-binding protein 2
PEBP1	Phosphatidylethanolamine-binding protein 1
PRC1	Protein regulator of cytokinesis 1
PRDX6	Peroxiredoxin 6
PRKAA1	Protein kinase AMP-activated catalytic subunit alpha 1
PRKAA2	Protein kinase AMP-activated catalytic subunit alpha 2
PRNP	Prion protein
RB1	RB transcriptional corepressor 1
RIPK1	Receptor interacting serine/threonine kinase 1
SAT1	Spermidine/Spermine N1-acetyltransferase 1
SAT2	Spermidine/Spermine N1-acetyltransferase family member 2
SESN2	Sestrin 2
SLC11A2	Solute carrier family 11 member 2
SLC39A14	Solute carrier family 39 member 14
SLC39A8	Solute carrier family 39 member 8
SLC3A2	Solute carrier family 3 member 2
SLC40A1	Solute carrier family 40 member 1
SLC7A11	Solute CARRIER FAMILY 7 MEMBER 11
SOCS1	Suppressor of cytokine signaling 1
STEAP3	STEAP3 metalloreductase
TF	Transferrin
TFRC	Transferrin receptor
TIGAR	TP53-induced glycolysis regulatory phosphatase
TP53	Tumor protein P53
VDAC1	Voltage-dependent anion channel 1
VDAC2	Voltage-dependent anion channel 2
VDAC3	Voltage-dependent anion channel 3

FRGs: Ferroptosis-related genes

TABLE S2. Twenty FRGs with the prognostic values determined by univariate Cox analysis

Gene	HR	Z	*p* value	Lower	Upper
SOCS1	1.657189491	4.677488875	2.90E-06	1.34106776	2.047828672
LPCAT3	1.454891425	4.068038933	4.74E-05	1.2144496	1.742936931
AIFM2	1.50920449	4.043975328	5.26E-05	1.236276341	1.842385975
GPX4	1.435587153	3.964423001	7.36E-05	1.20059353	1.71657636
SESN2	1.485639546	3.159234923	0.001581839	1.162143416	1.899184585
ACSL5	1.343501004	2.801010878	0.00509428	1.092711325	1.651849767
FH	1.335904392	2.685678401	0.007238272	1.081400517	1.650304875
GSS	1.34246805	2.639127694	0.008311967	1.078736361	1.670677406
FTH1	1.29210414	2.569986954	0.010170234	1.062718031	1.5710029
HSPB1	1.279328461	2.437135177	0.014804144	1.049412457	1.559616813
GOT1	1.270297676	2.283678418	0.022390437	1.034495825	1.559847943
G3BP1	0.761136109	−2.186344982	0.028790376	0.595934342	0.972134237
ACSL6	0.709078592	−2.182152893	0.029098251	0.520704331	0.965600668
CISD1	1.263085612	2.120941716	0.033926708	1.017884884	1.56735333
FTL	1.245546021	2.086044894	0.036974557	1.013359542	1.530932335
NFS1	1.270379737	2.082509115	0.037295991	1.014182154	1.591296661
MIF	1.197207319	2.064931186	0.038929512	1.009191547	1.42025106
CD44	0.771692716	−2.036828308	0.041667251	0.6013625	0.990267349
NCOA4	0.772211862	−1.973486003	0.048440218	0.597368269	0.998230391
SAT1	1.213835593	1.963969077	0.049533678	1.000395261	1.472814701

FRGs: Ferroptosis-related genes

TABLE S3. Twelve FRGs signature for OS generated by LASSO Cox regression analysis

Gene	Coef.	HR	Lower CI	Upper CI
ACSL6	−0.164270341	0.709078592	0.520704331	0.965600668
G3BP1	−0.05745754	0.761136109	0.595934342	0.972134237
CD44	−0.012600572	0.771692716	0.6013625	0.990267349
FH	0.011883347	1.335904392	1.081400517	1.650304875
GPX4	0.040188616	1.435587153	1.20059353	1.71657636
CISD1	0.070266332	1.263085612	1.017884884	1.56735333
SESN2	0.073905513	1.485639546	1.162143416	1.899184585
LPCAT3	0.074774143	1.454891425	1.2144496	1.742936931
AIFM2	0.075162582	1.50920449	1.236276341	1.842385975
ACSL5	0.115640755	1.343501004	1.092711325	1.651849767
HSPB1	0.184767081	1.279328461	1.049412457	1.559616813
SOCS1	0.287328369	1.657189491	1.34106776	2.047828672

FRGs: Ferroptosis-related genes, OS: Overall survival, LASSO: Least absolute shrinkage and selection operator

TABLE S4. Differential expressions of immune cell receptor-associated genes between low- and high-risk AML group

Gene	LogFC	AveExpr	t	*p* value	Adj. *p* value	B
ATP10D	2.983639618	6.993345222	4.21794539	4.61E-05	0.007055535	1.860897
GRB2	7.021457307	51.19749366	3.956956433	0.000124705	0.009539898	0.968567
BST2	−18.0461827	56.03778927	−3.838746368	0.000192902	0.009837977	0.578816
CFLAR	3.107276359	15.64680892	3.67791531	0.00034409	0.012989835	0.063473
MPZL1	4.802395249	11.12572483	3.58411036	0.000478386	0.012989835	−0.228969
SPCS3	8.123971631	34.53691739	3.56602947	0.000509405	0.012989835	−0.284636
PTRH2	1.657850975	6.774612264	3.512188573	0.000613386	0.013406865	−0.44905
CDC5L	2.657408038	11.82264652	3.334512016	0.001116209	0.020375051	−0.977039
CD160	0.894267388	2.492929048	3.312946058	0.001198532	0.020375051	−1.03958
EIF4A1	11.13616894	37.44252572	3.254755023	0.001449848	0.021998431	−1.206643
BCL2	6.916259365	12.70535223	3.200626531	0.001726954	0.021998431	−1.359809
TOX4	1.666857744	11.67299399	3.189025101	0.001792429	0.021998431	−1.392356
CD302	3.62903874	14.05407252	3.170970428	0.001898932	0.021998431	−1.442807
NOL11	4.311917669	15.7799086	3.139624884	0.002097911	0.021998431	−1.529822
SNURF	0.881139358	1.605562315	3.114565174	0.002270722	0.021998431	−1.598859
CD4	−11.59987764	27.05516844	−3.110428082	0.00230049	0.021998431	−1.610211
HNMT	−2.069733447	2.91626024	−2.881243139	0.004641443	0.040920534	−2.218771
VNN1	−6.641385608	11.8665279	−2.868953821	0.00481418	0.040920534	−2.250263
LTK	7.945209936	9.915484459	2.725143064	0.007321111	0.058954212	−2.60999
CD3G	0.998690742	2.47530472	2.701516728	0.007831402	0.059910223	−2.667528
C1QC	−8.34157969	7.670442615	−2.618144328	0.009899909	0.070418215	−2.867005
CD37	−12.35859263	63.02322699	−2.610029395	0.010125495	0.070418215	−2.886124
IFI16	8.750776122	35.92097568	2.585372489	0.010839614	0.070615464	−2.943888
C1QB	−12.07008409	9.345974219	−2.577501351	0.011076935	0.070615464	−2.962224
ACTR3	4.404088228	29.54609352	2.536126409	0.01240289	0.075905686	−3.057785
GBP3	1.342544628	6.128494966	2.49018311	0.014040388	0.082622282	−3.162265
SRA1	1.399237358	9.939609476	2.37334206	0.019105481	0.107756026	−3.420178
ABCD1	−1.42204049	8.003467474	−2.361100702	0.019720057	0.107756026	−3.446547
CEACAM8	4.6556822	3.604506278	2.343924579	0.02061181	0.108745065	−3.483336
SIGLEC1	−2.865282398	2.888490307	−2.320839431	0.021866292	0.111518091	−3.532394
TNFAIP2	−9.39660399	33.08851491	−2.273167168	0.024671299	0.121764797	−3.632295
BASP1	−6.978095906	14.58494698	−2.238756035	0.026887422	0.127053301	−3.703222
GPT2	3.742439436	8.067890707	2.224527818	0.027853385	0.127053301	−3.732258
CD3D	6.73086155	12.75292202	2.219038582	0.028234067	0.127053301	−3.743415
FLT3LG	0.3665493	1.220702718	2.164376243	0.032279103	0.141105794	−3.853121
CETN3	1.025807566	4.775143412	2.016082914	0.045870557	0.194949868	−4.137933
CCL23	−3.418882398	5.528213007	−1.965958753	0.051453508	0.212075245	−4.229931
RARA	−1.995181402	12.60440623	−1.955283066	0.052714183	0.212075245	−4.249245
FCGR3B	1.711198683	1.556195281	1.944135187	0.054058396	0.212075245	−4.269307
ZAP70	3.215609986	8.971397863	1.846557562	0.06710571	0.256679343	−4.440299
CCT6B	0.321745233	1.206086182	1.821102784	0.070911234	0.260926324	−4.483537
RAB1A	2.642850243	33.07099236	1.81644349	0.071626834	0.260926324	−4.49139
SIGLEC5	0.582983959	2.048906168	1.804866261	0.073430876	0.261277304	−4.51082
IL1RN	−1.399233035	4.519133082	−1.769075808	0.079247121	0.269748912	−4.570142
FN1	−1.570438822	2.533245883	−1.768534512	0.079337915	0.269748912	−4.571031
CTSZ	−10.30283048	68.13320681	−1.722044112	0.087461073	0.284173291	−4.646378
CD55	3.278509628	26.11461647	1.71841142	0.088123419	0.284173291	−4.652186
CDH2	1.019372651	1.224538929	1.712811789	0.089152405	0.284173291	−4.661114
SLC15A3	−0.889944692	2.785922821	−1.669638989	0.097418518	0.304184351	−4.729019
LIME1	0.590181599	2.748560726	1.646424252	0.10211335	0.312466851	−4.764847
WNT5B	−0.119892156	0.358574461	−1.576244848	0.117421424	0.352264272	−4.870238
ARHGAP10	0.574911504	2.103152447	1.545538845	0.124668508	0.366813109	−4.914964
CD300LB	−1.679023982	5.873486902	−1.452256321	0.14886105	0.418079047	−5.04564
FCER1G	−29.56449601	113.3818387	−1.449696213	0.14957286	0.418079047	−5.049116
CSE1L	4.018726888	32.22481682	1.447126951	0.150289854	0.418079047	−5.052598
ACAP1	2.546618532	21.6680036	1.364802111	0.174693767	0.477288329	−5.16101
FUCA1	−1.062497977	9.115158147	−1.354074466	0.178082662	0.478011357	−5.174684
CD69	18.98372835	65.49426441	1.313970866	0.191190492	0.504347331	−5.224873

(Contd....)

TABLE S4. *(Continued)*

Gene	LogFC	AveExpr	t	*p* value	Adj. *p* value	B
C3AR1	−4.634777598	21.81269706	−1.278882422	0.203236926	0.519702458	−5.267583
DPYD	2.133435083	13.55575856	1.277266463	0.203804886	0.519702458	−5.269523
HK3	−4.942301446	17.47403007	−1.262768092	0.208952967	0.524095147	−5.28682
PIK3IP1	−1.521949779	11.54836557	−1.237566391	0.218127297	0.535692205	−5.31643
GZMM	0.409354259	2.427337321	1.230962326	0.220579143	0.535692205	−5.324092
FASLG	0.091408071	0.412328331	1.177306524	0.241243239	0.563661532	−5.384866
EIF1	13.56765544	153.4541447	1.172891454	0.243003052	0.563661532	−5.389749
HLA−DPB1	−19.16295346	86.28485737	−1.172528538	0.243148112	0.563661532	−5.39015
GLS2	0.09797135	0.476500346	1.146024159	0.253909024	0.572369255	−5.419077
TREM1	−1.597846227	8.729331286	−1.144867058	0.254386336	0.572369255	−5.420325
FZR1	0.9120219	10.40251813	1.132240851	0.259635801	0.575714167	−5.433864
TREML4	0.226504517	0.786886262	1.101680889	0.272654039	0.595943829	−5.466025
LST1	−3.512748431	28.87885158	−1.08044392	0.281962668	0.607609693	−5.487867
FZD2	0.573786423	3.394969855	1.060976786	0.290685067	0.614048546	−5.507522
DAPP1	0.929380569	11.18369379	1.055926861	0.292977411	0.614048546	−5.512563
IGFBP5	0.4687394	1.639793821	1.032190023	0.303916587	0.618785535	−5.535943
SLC25A37	4.551982739	31.98930587	1.004575871	0.316983902	0.618785535	−5.562485
IGSF6	1.605334269	11.58674164	1.001902082	0.31826868	0.618785535	−5.565017
CD207	−0.047483413	0.068379246	−1.000677697	0.318858158	0.618785535	−5.566174
MS4A2	0.801248025	2.618466226	1.000222619	0.319077438	0.618785535	−5.566604
HAPLN3	−0.209467546	1.336266581	−0.999338699	0.319503642	0.618785535	−5.567439
GPR27	1.991649917	9.694418972	0.989264961	0.324387558	0.620391205	−5.576896
FPR1	−2.798528665	11.7003833	−0.950232117	0.343773238	0.63984849	−5.612649
GEMIN6	0.243418896	2.467798655	0.94982365	0.343979982	0.63984849	−5.613015
CD3E	1.597737329	11.074917	0.943664123	0.347107351	0.63984849	−5.618526
CXCL1	0.404814341	1.56981927	0.921214056	0.358660244	0.642590406	−5.638309
SLAMF9	0.102709888	0.379234006	0.916393463	0.361172489	0.642590406	−5.642496
DAXX	−0.839219232	18.10358162	−0.911061686	0.363964107	0.642590406	−5.647102
RHOA	22.09015536	291.4114678	0.908339684	0.365394544	0.642590406	−5.649443
SLA	−1.079593815	13.58861955	−0.8976344	0.371054651	0.64512911	−5.658583
TNFRSF11A	0.116694263	0.572631388	0.888915548	0.375704938	0.645874781	−5.665948
FAM198B	−1.007429432	5.619501756	−0.864526182	0.388905488	0.661139329	−5.686173
AXL	0.16558146	0.752210297	0.854202251	0.394578245	0.663411774	−5.694567
UBA52	4.276503066	83.43556134	0.825418139	0.410659816	0.677912535	−5.717444
FKBP4	2.536919016	21.82775182	0.822936542	0.412064482	0.677912535	−5.719379
GLUD1	2.043995266	40.42321789	0.800668525	0.424797398	0.691425551	−5.736493
GUSB	−1.689825646	27.58753062	−0.780219372	0.436692647	0.703305001	−5.7518
CRYBB1	0.191414207	1.073469866	0.771185798	0.442008688	0.704451346	−5.758437
DGKH	−0.145823562	0.984770735	−0.742726076	0.458999448	0.723988821	−5.778847
GM2A	−0.905333608	21.22931697	−0.719365785	0.473218244	0.732072991	−5.795031
TREML1	0.314365504	1.505208031	0.71859053	0.473694288	0.732072991	−5.795559
CCL14	0.036857667	0.140573826	0.6919286	0.490227107	0.748135928	−5.813384
TRIB2	0.75754883	3.673946015	0.686124251	0.493867508	0.748135928	−5.817176
CD8A	0.329425653	3.325966438	0.677701883	0.499175813	0.748763719	−5.822622
FCRL6	0.235466079	2.065618556	0.660886398	0.509865058	0.757372368	−5.833295
ATP6V1A	0.818616301	24.07506287	0.648325198	0.517928322	0.761034536	−5.841094
HLA-DPA1	−5.249501113	52.85141603	−0.631460692	0.528857975	0.761034536	−5.851331
NPL	−0.449777839	3.828592113	−0.6290957	0.530400135	0.761034536	−5.852746
F11R	0.863612566	13.74178175	0.623336268	0.534165375	0.761034536	−5.856168
NTRK1	−0.295268684	1.530780842	−0.618708196	0.537200849	0.761034536	−5.858895
NKG7	5.03275304	69.62243967	0.585439622	0.559276072	0.78503889	−5.877903
IL2RB	0.764375906	7.250086143	0.542495741	0.588414095	0.812396432	−5.900896
C1GALT1C1	0.363247194	11.5063196	0.541081478	0.589385647	0.812396432	−5.901623
TIMM13	−0.710660782	15.55453603	−0.525900993	0.599860941	0.819452893	−5.909314
GNLY	−1.188619192	9.658534938	−0.507275523	0.612828616	0.825713475	−5.918452
HLA−DMB	−1.046014194	14.67654637	−0.499655783	0.618169611	0.825713475	−5.922096
TNFSF14	0.133975949	1.659016278	0.4958237	0.620863438	0.825713475	−5.923908
CAPG	1.897007596	33.2061004	0.481565768	0.630931304	0.825713475	−5.930527
ADCY9	−0.311146701	4.971593848	−0.474182361	0.636172427	0.825713475	−5.933879

(Contd....)

TABLE S4. *(Continued)*

Gene	LogFC	AveExpr	t	*p* value	Adj. *p* value	B
FRMD4A	0.135908115	1.558911661	0.473265199	0.636824771	0.825713475	–5.934292
CSF2RA	–0.823421781	15.92476078	–0.458458558	0.647395337	0.827820006	–5.940846
VNN2	–1.768682445	10.38140047	–0.455842429	0.649270593	0.827820006	–5.941982
RNASE2	–14.8980131	302.0010428	–0.445695895	0.656564891	0.830201887	–5.946328
FPR2	–0.300546408	2.834862212	–0.436445301	0.663244108	0.831773348	–5.950206
SIK1	0.050025859	0.412959452	0.417109161	0.677292673	0.842486007	–5.958049
SETD7	0.180009269	3.299292795	0.39726685	0.691827979	0.853626458	–5.965729
AHSA1	–0.489123146	22.15753258	–0.379474117	0.704960487	0.861390126	–5.972298
CCNA1	2.101718486	22.48756951	0.370914222	0.711310526	0.861390126	–5.975351
XPO6	–0.412225332	25.48063312	–0.365939789	0.715010105	0.861390126	–5.977094
CMKLR1	–0.088413227	1.273306054	–0.348719151	0.727869316	0.863442747	–5.982945
CCR5	–0.195126918	2.755072596	–0.348543689	0.728000747	0.863442747	–5.983003
KANK2	0.222743751	5.364595853	0.324283814	0.746248996	0.878277665	–5.990764
CRTAM	–0.028047408	0.837657823	–0.30294733	0.762418543	0.882271169	–5.997128
AKT3	0.324196272	4.423456809	0.298113674	0.766096571	0.882271169	–5.998509
APOL3	–0.177612997	5.250477964	–0.297004128	0.766941604	0.882271169	–5.998823
FRAT2	0.309298482	14.36019835	0.27615201	0.782873741	0.893878227	–6.004507
CCL1	0.180177997	1.738176698	0.257481631	0.797217734	0.903513432	–6.009246
FES	–0.684290218	45.46381532	–0.239650565	0.810981966	0.912354712	–6.013463
LCK	0.172828618	5.254391526	0.222990135	0.823896293	0.920117758	–6.01713
ADRM1	0.44432581	23.81582382	0.170673344	0.864748332	0.9525595	–6.026928
FAM49A	0.146074454	7.913120657	0.16950379	0.865666216	0.9525595	–6.027117
FSTL1	0.074158614	1.742515692	0.16191925	0.871623072	0.9525595	–6.028313
GZMK	0.065175162	2.733442692	0.144172425	0.885589561	0.956633168	–6.030898
F13A1	–1.460954224	47.96099279	–0.13472479	0.893039692	0.956633168	–6.032152
ACTN4	–0.684484596	84.3035886	–0.126235782	0.899742051	0.956633168	–6.033206
GZMH	–0.102936751	4.316010468	–0.120068783	0.904615674	0.956633168	–6.033929
AIF1	0.755609594	91.65033351	0.108543824	0.913733166	0.956633168	–6.035183
BCL2L1	0.188626067	15.23047054	0.103430316	0.917782259	0.956633168	–6.035698
CNR2	0.032612827	1.602347177	0.101743864	0.919118142	0.956633168	–6.035863
CYTH1	0.086613874	19.37875002	0.08317087	0.933844744	0.960705126	–6.037497
FCGR1A	–0.044619459	3.951520895	–0.080973514	0.935588652	0.960705126	–6.037669
NFKBIA	–0.317402225	54.09037709	–0.058599336	0.953362021	0.971392295	–6.039155
HLA-DQA2	–0.118878748	8.326919021	–0.051892947	0.958694357	0.971392295	–6.039508
CLEC4C	–0.040291985	2.116219877	–0.030068662	0.976058817	0.982480257	–6.040359
GZMA	–0.012285773	7.381601484	–0.011111064	0.991152021	0.991152021	–6.040731

AML: Acute myeloid leukemia

TABLE S5. Differential expressions of immune regulatory genes between high- and low-risk AML group

Gene	LogFC	AveExpr	t	*p* value	Adj. *p* value	B
B2M	82.2876106	642.9617947	2.588448744	0.010750536	0.129006429	–3.020887
CD96	41.30678947	53.07271838	3.366367029	0.001004799	0.023583141	–0.93992
TAPBP	11.66245463	75.46683206	2.108022821	0.03697013	0.233495561	–4.061621
CD244	11.59442811	27.52892359	4.008205384	0.000103032	0.012363869	1.113176
TGFBR1	4.701133677	13.33543564	3.318056076	0.001179157	0.023583141	–1.082635
NT5E	1.786249779	2.123888517	2.230614111	0.027440276	0.193696069	–3.814636
MICB	1.400588663	10.15747527	2.043188529	0.043076971	0.247165032	–4.186993
CD160	1.041031771	2.590629612	3.476694659	0.000692967	0.020789003	–0.60761
CD28	0.997874598	1.685008989	3.548643816	0.000541377	0.020789003	–0.386166
CXCL17	0.57286768	1.254964334	2.402721093	0.017702221	0.151733322	–3.446259
CXCR6	0.517944252	1.541759554	2.858159141	0.004972321	0.066297613	–2.353006
KLRK1	0.41068442	0.50886	2.415500572	0.017119623	0.151733322	–3.417909
ICOS	0.362274173	0.906801892	2.929508408	0.004017959	0.060269379	–2.166611
TIGIT	0.251186364	0.719548732	3.672583671	0.000350918	0.020789003	0.003901
ADORA2A	0.149914254	0.541535294	2.268615714	0.024958518	0.193696069	–3.735459
CCR10	–0.157773164	0.398541325	–1.995370105	0.048116251	0.259687358	–4.277116
CD80	–0.343439686	0.543279938	–2.041430866	0.043253881	0.247165032	–4.190341

(Contd....)

TABLE S5. *(Continued)*

Gene	LogFC	AveExpr	t	*p* value	Adj. *p* value	B
CD40	−0.633402573	2.158345669	−2.461267362	0.015170354	0.151733322	−3.315261
IL10	−0.790521921	0.762128475	−2.459028998	0.015260882	0.151733322	−3.320322
IL2RA	−4.075148214	4.9424882	−1.980576273	0.04977341	0.259687358	−4.304592
CCR1	−4.936609138	12.70066637	−2.160931283	0.032554065	0.217027101	−3.956612
HLA-DMA	−9.688738118	51.39603482	−2.240357846	0.026784231	0.193696069	−3.794452
HLA-B	−67.1675588	389.9494837	−3.019536822	0.003054119	0.052356329	−1.925733
TMIGD2	3.236569207	8.662754619	1.907029325	0.058747629	0.293738147	−4.438338
TNFSF18	−0.031936578	0.054242246	−1.882949461	0.061966568	0.297439524	−4.481092
CCL13	0.055093702	0.100834204	1.847102897	0.067031	0.309373848	−4.543786
CXCL11	−0.054151264	0.083986335	−1.775658251	0.078154903	0.347355124	−4.665334
CCL23	−3.778460272	6.509334707	−1.723632342	0.08717791	0.365882467	−4.750979
CCR9	0.273349877	0.771593779	1.709529602	0.089765232	0.365882467	−4.773777
CXCL8	15.31770101	26.40166837	1.69171958	0.093121702	0.365882467	−4.802312
CCL5	−5.907386304	27.87008936	−1.68445545	0.094519637	0.365882467	−4.813869
HLA-DQB1	−6.194074281	23.49734816	−1.618629969	0.10797734	0.404915026	−4.916426
CD48	3.457735563	18.09234061	1.599386482	0.11218918	0.407960656	−4.945667
TAP2	1.44235251	9.801615725	1.549074804	0.12382165	0.437017588	−5.020532
CCR3	0.146326466	0.345955607	1.517655618	0.131556167	0.44271731	−5.066117
TNFSF13	−1.17606766	7.318239029	−1.489941377	0.138688632	0.44271731	−5.10558
TNFRSF13C	0.746305786	3.415562238	1.48852894	0.13906005	0.44271731	−5.107573
CXCL10	−0.378148546	0.823512327	−1.484235537	0.140193815	0.44271731	−5.113618
IDO1	0.057109697	0.087296738	1.417459979	0.158767224	0.474958583	−5.205466
CCL4	−0.554575168	2.534080008	−1.408419256	0.161420444	0.474958583	−5.217587
CD276	−0.463899911	1.174002391	−1.389790108	0.166994258	0.474958583	−5.242327
TNFSF4	2.835418363	7.040436039	1.384174311	0.168702882	0.474958583	−5.249722
LAG3	−0.603660015	1.293810335	−1.379310229	0.170193492	0.474958583	−5.256104
ENTPD1	1.327937512	8.171825098	1.307259007	0.19345768	0.527611856	−5.348082
CCL3	−0.662441788	2.663485752	−1.278307292	0.203443845	0.542516921	−5.38369
CXCL1	0.640473883	1.686329072	1.258536924	0.210478054	0.545084995	−5.407559
CCL14	0.048007845	0.143597427	1.249159501	0.213876078	0.545084995	−5.418754
CD274	−0.153797844	0.517762402	−1.237831772	0.218033998	0.545084995	−5.432169
HHLA2	0.147505917	0.515463243	1.183883676	0.238643162	0.584432235	−5.494416
CD70	−0.902567486	1.969503985	−1.140345251	0.25626219	0.608284417	−5.542676
CCL18	−0.241562673	0.521995977	−1.134918206	0.258520877	0.608284417	−5.548567
CXCR1	0.322605956	0.82763661	1.110654995	0.268789563	0.617393181	−5.57457
KDR	0.073046622	0.250104506	1.100313217	0.273251421	0.617393181	−5.585486
TAP1	1.84211873	17.75892984	1.089828634	0.277826932	0.617393181	−5.59645
CD40LG	0.467113821	2.105116742	1.071728094	0.285849694	0.623672059	−5.615137
CCL20	−0.043635229	0.104284834	−0.983150243	0.327379876	0.701528305	−5.702146
LGALS9	−2.719177775	30.41985139	−0.967775778	0.334973228	0.705206795	−5.716497
CXCL16	−0.75973126	3.618589007	−0.918233791	0.360215759	0.724338628	−5.761222
TNFRSF4	2.592201158	5.952644875	0.913943563	0.36245717	0.724338628	−5.764987
CCL21	−0.05025765	0.127509469	−0.906081896	0.366587341	0.724338628	−5.771839
CXCL5	−0.185016031	0.220483718	−0.900819547	0.369368467	0.724338628	−5.776393
TNFRSF14	1.56638799	14.42375357	0.891658457	0.374241624	0.724338628	−5.784259
HLA-DRA	−43.47862458	545.4995157	−0.864976158	0.388662822	0.725867639	−5.806717
CCR5	−0.428162152	2.59873829	−0.862528535	0.390002639	0.725867639	−5.808743
CXCL12	4.21335147	15.20142419	0.855458758	0.393888525	0.725867639	−5.814564
HLA-DRB1	−17.42490842	180.0543118	−0.845815126	0.399227202	0.725867639	−5.822428
TGFB1	−6.807297851	91.58364481	−0.819577836	0.413973442	0.741444971	−5.843377
TNFSF14	0.229721163	1.743311516	0.775336317	0.439564607	0.775702247	−5.877222
HLA-DQA1	−1.521333384	10.60929612	−0.753614144	0.452458751	0.786884784	−5.893159
IL6R	1.960401826	31.03493488	0.721918815	0.471655242	0.78778896	−5.915608
HLA-DOA	−1.048611291	7.762181609	−0.717158929	0.474576837	0.78778896	−5.918897
HAVCR2	0.609502217	7.458584666	0.714242146	0.476372103	0.78778896	−5.920901
HLA-A	−10.88939198	217.0917724	−0.709598032	0.479238284	0.78778896	−5.924076
HLA-DPB1	−5.861241008	68.42972642	−0.688889874	0.492133777	0.798054773	−5.937984

(Contd....)

TABLE S5. *(Continued)*

Gene	LogFC	AveExpr	t	*p* value	Adj. *p* value	B
CCR2	1.926666031	11.90532807	0.641019223	0.522651108	0.811283189	–5.968568
CCL1	0.705734899	2.368668143	0.627752968	0.531279105	0.811283189	–5.976657
CD86	–0.854038844	8.347567501	–0.613546573	0.540598899	0.811283189	–5.985133
BTLA	0.624461411	2.958924156	0.602399396	0.547969223	0.811283189	–5.991648
HLA-E	9.104142691	225.5157774	0.594856923	0.552984521	0.811283189	–5.995989
CCL25	0.093898696	0.407753268	0.585669519	0.559124201	0.811283189	–6.001204
TNFRSF8	–0.092359608	0.929804067	–0.581785139	0.561730055	0.811283189	–6.003384
CXCL3	–0.312119564	2.236655835	–0.567988709	0.571033175	0.811283189	–6.011012
HLA-G	0.157236533	2.149249118	0.555944066	0.579215236	0.811283189	–6.017522
LTA	0.031479835	0.487891202	0.551961257	0.581933003	0.811283189	–6.019644
HLA-DPA1	–3.420234631	44.38800217	–0.549693894	0.583482881	0.811283189	–6.020845
CCR7	0.526838963	6.371294579	0.525489329	0.600148127	0.811283189	–6.033363
HLA-DQA2	–0.949727564	7.51284808	–0.507266698	0.612836646	0.811283189	–6.042417
TNFSF13B	2.519286962	41.96448329	0.505378965	0.614157913	0.811283189	–6.043337
XCL2	–0.074796026	0.958019119	–0.501794331	0.616670367	0.811283189	–6.045074
XCL1	0.022679138	0.28385469	0.497767855	0.619497931	0.811283189	–6.04701
CXCR3	–0.169456748	1.915101532	–0.488149461	0.62627541	0.811283189	–6.051573
HLA-C	–6.06390577	214.8258794	–0.484536103	0.628829833	0.811283189	–6.053265
CXCL9	–0.118191777	0.427300327	–0.481011	0.631326205	0.811283189	–6.054903
CD27	0.249467915	4.774824006	0.462137269	0.644763913	0.811283189	–6.063469
CCR4	0.077600602	0.957032015	0.442456454	0.658902333	0.811283189	–6.072039
CCL24	–0.337385646	1.19363008	–0.433091197	0.665674166	0.811283189	–6.075986
CTLA4	–0.034897019	0.6699576	–0.431538309	0.666799719	0.811283189	–6.076632
CCL17	0.011063288	0.095699268	0.428954666	0.668674057	0.811283189	–6.077703
CXCR4	–8.696111762	143.1828419	–0.428080605	0.669308631	0.811283189	–6.078063
CCL2	–0.032154359	0.244128242	–0.402495741	0.687987596	0.825585115	–6.088294
CX3CR1	–2.790529335	25.28864878	–0.380995461	0.7038354	0.836240079	–6.096406
CSF1R	2.024802395	42.88481943	0.34076338	0.733837878	0.860422982	–6.110391
HLA-F	0.347338604	9.903972299	0.324767628	0.745884748	0.860422982	–6.115519
TNFSF9	–0.231173074	2.534870685	–0.317129513	0.751659696	0.860422982	–6.117881
CXCR2	0.189628201	2.877752729	0.310576627	0.756625386	0.860422982	–6.119863
TNFRSF18	–0.549311511	3.485795228	–0.306077993	0.760040301	0.860422982	–6.121199
PVR	0.444062533	9.541057132	0.264704228	0.791661182	0.88010786	–6.132577
TMEM173	2.584053042	75.71745716	0.264137231	0.792097074	0.88010786	–6.132722
PDCD1LG2	–0.01608263	0.384289048	–0.247449934	0.804954737	0.886188701	–6.136835
CCL28	0.080736103	2.496019623	0.19242232	0.847714997	0.924779997	–6.148501
IL10RB	0.386033642	23.957728	0.171339217	0.864226403	0.929580527	–6.152197
PDCD1	0.062134636	1.431204449	0.155690808	0.876520908	0.929580527	–6.154664
HLA-DOB	0.05027201	3.224243081	0.14364465	0.886005966	0.929580527	–6.156402
TNFRSF13B	0.006581983	0.326440024	0.130247155	0.896574439	0.929580527	–6.158171
TNFRSF17	–0.107385824	2.992409092	–0.125572538	0.900266435	0.929580527	–6.158748
HLA-DMB	–0.194402454	13.34194268	–0.120627209	0.904174614	0.929580527	–6.159335
CXCL14	0.010812926	0.283355	0.112599357	0.910523801	0.929580527	–6.160237
CXCL2	0.218573022	9.345557121	0.108096662	0.914087519	0.929580527	–6.160716
CCL8	0.002785634	0.068279609	0.074441185	0.940775029	0.948680701	–6.163678
TNFRSF25	0.047024686	5.532516894	0.044508464	0.964568155	0.964568155	–6.165395

AML: Acute myeloid leukemia